İSTANBUL UNIVERSITY CERRAHPAŞA

ORIGINAL ARTICLE
Electrica 2025; 25: 1-20

Asynchronous Motor Bearing Fault Diagnosis and Speed Control Using Fuzzy Logic-Based Direct Torque Controller

Abderrahman El Idriss[1], Aziz Derouich[1], Said Mahfoud[2], Najib El Ouanjli[3], Ahmed Chantoufi[1], Mohamed I. Mosaad[4]

[1]Industrial Technologies and Services Laboratory, Higher School of Technology, Sidi Mohamed Ben Abdellah University, Fez, Morocco
[2]Polydisciplinary Laboratory of Sciences, Technologies, and Societies, Higher School of Technology, Sultan Moulay Slimane University, Khenifra, Morocco
[3]Laboratory of Mechanical, Computer, Electronics, and Telecommunications, Faculty of Sciences and Technology, Hassan First University, Settat, Morocco
[4]Department of Electrical and Electronics Engineering Technology, Royal Commission Yanbu Colleges and Institutes, Yanbu Industrial City, Saudi Arabia
The sections of this article are structured as follows: The ASM model is shown in Section 2. Section 3 presents the three BFs and their distinctive frequencies. The FL-DTC control is the subject of Section 4. Section 5 gives an overview of the HT. Section 6 presents and interprets the results, and Section 7 finishes this work.

Cite this article as: A. E. Idriss, A. Derouich, S. Mahfoud, N. El Ouanjli, A. Chantoufi, and M. I. Mosaad, "Asynchronous motor bearing fault diagnosis and speed control using fuzzy logic-based direct torque controller," *Electrica*, 25, 0121, 2025, doi: 10.5152/electrica.2025.24121.

ABSTRACT

Asynchronous motors (ASMs) have attracted significant attention due to their extensive use in industrial applications and processes, particularly when it comes to adjusting speeds. Several speed control methods, including fuzzy logic-direct torque controller (FL-DTC), have been suggested to regulate the speed of ASMs by accurately following the desired reference speed. The fluctuating reference speed directly influences the operational frequency of the ASM stator current, a critical factor in the identification of bearing faults (BFs). Notably, BFs contribute to 40% of all ASM failures. This article describes the detection of BFs in ASMs via a combination of the Hilbert transform (HT) and the FL-DTC. Hilbert transform is employed to analyze the non-stationary nature of the stator's current with speed variations. These variations come in two forms: those caused by the control itself and those resulting from BFs. The FL-DTC control contributes to reducing current harmonics, torque, and speed ripples. This highlights and makes the effects induced by BFs more distinct, thus rendering them more proportional. As such, the FL-DTC control is not only employed to enhance the performance of the ASM, but it is also utilized for the diagnosis of BFs. The performance of the selected approach is tested in the MATLAB/Simulink environment.

***Index Terms*—**Asynchronous motor (ASM), bearing fault (BF), fuzzy logic-direct torque controller (FL-DTC), Hilbert transform (HT), motor current signature analysis (MCSA)

Corresponding author:
Said Mahfoud

E-mail:
said.mahfoud@usmba.ac.ma

Received: September 23, 2024

Revision requested: November 22, 2024

Last revision received: December 16, 2024

Accepted: December 23, 2024

Publication Date: January 27, 2025

DOI: 10.5152/electrica.2025.24121

I. INTRODUCTION

Compared to direct current (DC) and synchronous machines, asynchronous motors (ASMs) are employed in many more applications because of the tremendous advancements and dramatic cost reduction in power electronics [1, 2]. These uses are not just for motors but also for generators, particularly for wind applications, with the two well-known types being self-excited and doubly fed induction generators [3–5]. Particularly for the squirrel cage type, ASMs are distinguished by their simple structure, controllability, and low maintenance requirements. In reality, because of their extensive usage, ASMs now perform essential tasks, necessitating higher levels of dependability as well as the need to maintain high levels of production. As a result, while using ASM in the majority of applications, two key factors, defect diagnosis and control, must be taken into account.

From a control standpoint, the induction motors' speed should be controlled since load fluctuations have an impact on it. Many research projects improve the control strategies for electric machines. The first one is the scalar control (SC) [6], which has an open-loop control unit and is highly well-liked in the industry. However, at low speeds, the machine parameters become non-negligible, causing a voltage drop for this regime. The second is vector control, which includes many types and seeks to be improved. Direct flux orientation control (DFOC) requires the implementation of flux sensors in the motor air gap. The indirect flux control (IFOC) overcomes the use of using these sensors in DFOC. The reliability and stability of the systems, however, cannot be guaranteed by IFOC. Sliding mode control (SMC) was designed to increase stability and

WHAT IS ALREADY KNOWN ON THIS TOPIC?

- *Asynchronous motors (ASM) are commonly used in industrial applications that require precise speed control.*
- *Several speed control methods such as Fuzzy Logic - Direct Torque Controller (FL-DTC) have been proposed to control the ASM speed by precisely following the desired reference speed.*
- *Bearing failure (BF) is a leading cause of ASM failures, accounting for approximately 40% of all failures.*
- *Speed variations affect the stator current frequency, which can be used to detect BFs.*
- *Closed-loop controls such as DTC cause current non-stationarity, which calls for the use of advanced signal processing methods such as Hilbert Transform to diagnose broken rotor bars.*
- *Enhanced DTC control by the neural network with the adoption of Hilbert Transform is also effective in helping to diagnose BFs.*

WHAT THIS STUDY ADDS ON THIS TOPIC?

- *This study introduces a combination of Hilbert transform (HT) with FL-DTC method for BF detection in ASM. It is emphasized that FL-DTC control not only improves efficiency by reducing current harmonics, torque and speed waves. But it also expands the effect of BF, making detection easier. It demonstrates the ability of this integrated approach to optimize ASM and facilitate bearing fault diagnosis. especially in the phase of confirmation and precise localization of BF. Also, even if a high-performance control can compensate for the effect of faults on the current, but according to studies it can also better distinguish spectra indicating mechanical-type faults such as BFs. Essentially, the added contributions are the detection of the three bearing faults on the MAS (inner ring, outer ring, ball), taking advantage of the presence of DTC control enhanced by fuzzy logic and the Hilbert transform.*

dependability. However, it results in the "Chattring" phenomenon, a high-frequency vibration that degrades the machine's life. The direct torque control (DTC) proposed by Takahashi [7] and Depenbrock [8] presents the best-performing solution. The main advantages of this strategy lie in its robustness, simplicity, and limited sensitivity to machine parameter variation. Yet, its primary drawback is flux and torque ripples that produce acoustic noise and mechanical vibrations [9, 10, 11–13]. To improve the effectiveness of the DTC control in this respect, researchers used artificial intelligence (AI) to minimize the torque ripples [9, 12–14]. Artificial neural networks (ANNs) was presented to support the DTC, and ANN-DTC in ASM [12, 13]. The results demonstrate that the ASM stator current's performance in terms of flux and torque profiles as well as total harmonic distortion (THD) has improved [12, 13]. Fuzzy logic (FL) was integrated into the DTC control to develop a new FL-DTC control. In this combination, FL-DTC substitutes the hysteretic comparators and the switching table with affuzzy logic controller to simplify the structure of the controller [14–16]. The authors have demonstrated that this intelligent control offers better performances in terms of electromagnetic torque, rotational speed, and THD of line current.

While from the diagnoses standpoint, a failure in one of the machine's components can stop the whole production process, resulting in significant financial losses [17]. The faults within the ASMs can be classified into three groups: electrical faults in the stator (38%), electrical faults in the rotor (10%), and bearing faults (BFs) (40%); the other faults represent about 12% [18].

Both the manufacturers and the users of electrical machines have already installed basic protections against overcurrents, overvoltages, isolation failures, etc. While the tasks performed by these protections were not always easy, they were critical. As the sophistication of these machines' tasks increased, so did the requirement for enhancements in fault detection. From this review, bearing faults (BF) is the most frequent fault in ASM. The early stages of these issues are usually identified and diagnosed via vibration monitoring. However, this method is extremely expensive and challenging since the interpretation of vibration signals calls for specialist equipment, specialized knowledge, and a complete understanding of certain mechanics [19–21]. The most widely used technique for identifying BFs as an alternative to mechanical techniques is motor current signature analysis (MCSA). This is so because currents are simple to measure and can reveal a variety of faults.

By using the Fast Fourier Transform (FFT), MCSA may provide specialized spectra that can be used to identify certain ASM faults [22–24]. But for the researchers, the non-stationarity of the current signal and the continuous variation of the rotational speed represent a great challenge. If the ASM drives use an inverter or a closed-loop control such as a DTC, the current is no longer constant, thus making it more challenging to use an FFT that is sufficient to process it.

To address the problem of non-stationary signals, advanced signal processing methods present a more effective solution. Several techniques, including the wavelet transform (WT) [25] or discrete wavelet transform (DWT) [26], the Hilbert transform (HT) [20, 25, 27, 28], and the short-term fourier transform (STFT) [14], are used to diagnose faults in electrical equipment with non-stationary signals.

The HT-based approach has proven to be effective for both vibration signal analysis and current signal analysis [19]. The main key features of HT benefits of this transform are its low sensitivity to fluctuations in load torque and the simplicity of its mathematical model [10, 29]. In ref. [10], the HT was used for broken rotor bars (BRBs) detection in an ASM controlled by DTC. Additionally, HT was preferred by the authors for the diagnosis of BRBs in ASM as concluded in ref. [24]. A hybrid technique based on DWT and HT is developed in ref. [2] for identifying and categorizing different ASM faults and is also used in combination with FFT for the detection of induction machine outer race BF in ref. [30]. This technique is effective in identifying faults in the ASMs fed by inverters where the line current is non-stationarity. Therefore, machine control must be considered when selecting diagnostic procedures. For the BFs' accuracy and diagnostic effectiveness, the rotational speed signal quality is crucial as the rotational frequency has a significant influence on the harmonic spectra [31]. Even in the presence of BFs or minor load torque fluctuations, the control must function effectively and robustly, following the reference speed.

The aim of this work is to explore the use of FL-DTC for the diagnosis of BFs ASMs, and its primary role in improving its performance. The process involves reducing the amplitudes of electric current harmonics, including those caused by BFs. However, the ratio of the amplitudes of the BF spectrum to the fundamental frequency increases, allowing more accurate detection of BFs from the current spectrum, particularly when the fault frequency is higher than the fundamental.

This distinction in the spectrum can help to improve the accuracy of future intelligent classification of BFs based on electrical current data.

In addition, the HT is designed to extract the frequency spectra generated by the BFs independently of the variation in supply frequency, resulting directly in fault location. The following is a summary of this paper's important contributions:

- Create an FL-DTC control to minimize rotation speed deviations and to follow the reference speed, whose value allows the extraction of the BFs' characteristic frequencies.
- Torque ripples are reduced by more than half when compared to traditional DTC.
- A comparison of results obtained using direct fed (DF), traditional DTC, and FL-DTC.
- Spectral analysis of the stator current envelope (SSCE) of the ASM by HT and FFT.
- Diagnosis of the three types of BFs.

II. ASYNCHRONOUS MACHINE MODEL

In this study, the BFs modeling is implemented in the mechanical part, which concerns the load torque. Therefore, a basic model of the ASM is useful. The ASM's nonlinear system, which is characterized by electromagnetic and mechanical parameters, may be represented by the following equations [28]:

- Electrical equations:

$$\begin{cases} v_{s\alpha} = R_s.i_{s\alpha} + \dfrac{d\psi_{s\alpha}}{dt} \\ v_{s\beta} = R_s.i_{s\beta} + \dfrac{d\psi_{s\beta}}{dt} \\ 0 = R_r.i_{r\alpha} + \dfrac{d\psi_{r\alpha}}{dt} + \omega_m.\psi_{r\beta} \\ 0 = R_r.i_{r\beta} + \dfrac{d\psi_{r\beta}}{dt} - \omega_m.\psi_{r\alpha} \end{cases} \quad (1)$$

- Magnetic equations:

$$\begin{cases} \psi_{s\alpha} = L_s i_{s\alpha} + L_m.i_{r\alpha} \\ \psi_{s\beta} = L_s i_{s\beta} + L_m.i_{r\beta} \\ \psi_{r\alpha} = L_r i_{r\alpha} + L_m.i_{s\alpha} \\ \psi_{r\beta} = L_r i_{r\beta} + L_m.i_{s\beta} \end{cases} \quad (2)$$

- Mechanical equations:

$$\begin{cases} T_m = p.(\psi_{s\alpha} i_{s\beta} - \psi_{s\beta} i_{s\alpha}) \\ J.\dfrac{d\Omega}{dt} + f.\Omega = T_m - T_r \end{cases} \quad (3)$$

III. BEARING FAULTS

A bearing is used to guarantee the rotational guidance for shafts in rotating machinery and prevent any other movement except rotation. Ball bearings are the most standard, as shown in Fig. 1. They consist of the balls (Ball), inner race (IR), outer race (OR), and the cage or train. Electrical machines usually have two bearings by which the ends of the rotor shaft are held.

Bearing faults generally cause vibrations, increases in the sound level emitted by the machine, and rotor eccentricity, which results in a magnetic attraction that is not balanced. Additionally, they cause harmonics in the current signal and oscillations in the load torque of the machine [9, 20, 25, 31].

Bearing condition monitoring techniques based on current analysis or vibration analysis are developed to detect and locate the three specific fault frequencies, namely IR, OR, and ball [27, 30].

Bearing dimensions and machine rotation frequency determine the values of the characteristic frequencies [22, 27, 30].

- Frequency of bearing outer race fault:

$$f_{OR} = \frac{N_b}{2} f_r \left(1 - \frac{D_b}{D_c}\cos\alpha\right) \quad (4)$$

- Frequency of bearing inner race fault:

$$f_{IR} = \frac{N_b}{2} f_r \left(1 + \frac{D_b}{D_c}\cos\alpha\right) \quad (5)$$

- Frequency of bearing ball fault:

$$f_{Ball} = \frac{D_c}{2D_b} f_r \left[1 - \left(\frac{D_b}{D_c}\cos\alpha\right)^2\right] \quad (6)$$

The corresponding frequency of the BFs is obtained by the following equation [27, 32, 33]:

$$f_d = f_s \pm k.f_c \quad (7)$$

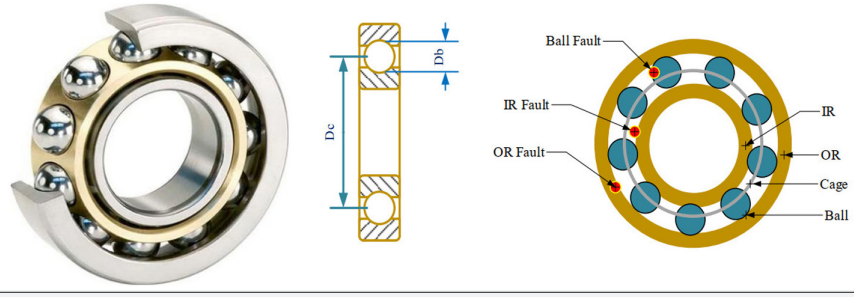

Fig. 1. Composition of a ball bearing and location of the bearing faults.

k: Harmonic's order.

The BFs cause oscillations in the load torque, which allows us to model them by (8), where a constant component is expressed by amplitude T_0 and BF-related torque oscillations by amplitude T_c and frequency f_c are used to express the load torque [34].

$$T_r(t) = T_0 + T_c.\cos(2\pi f_c.t) \tag{8}$$

IV. DIRECT TORQUE CONTROL BASED ON FUZZY LOGIC

Direct torque control is one of the most popular controls in the industry [10] because of its improved torque dynamics and robustness. Still, its main disadvantage is the torque and flux ripples caused by hysteresis comparators [14], which cause audible noise and mechanical vibrations that reduce machine life [9].

To overcome these problems and improve the performance of this control, researchers are incorporating AI into their work to design a new, more robust, and better-performing intelligent DTC strategy. The replacement of hysteresis comparators and switching tables by FL-based controllers are among the solutions adopted in this regard in several research works [14–16].

A. Classical direct torque control

Direct torque control has become very popular and was initially introduced in the 1980s by Depenbrock and Takahashi [7, 8]. This strategy is based on the use of hysteresis comparators and control quantity estimates of electromagnetic torque and stator flux. The estimates are determined from the voltages and electric currents of the ASM lines (Eqs. 9 and 10), with no need for flux sensors positioned in the machine air gap [9, 11].

- The estimated flux:

$$\begin{cases} \psi_{s\alpha\text{-est}} = \int \left(v_{s\alpha} - R_{s\alpha} i_{s\alpha}\right) dt \\ \psi_{s\beta\text{-est}} = \int \left(v_{s\beta} - R_{s\beta} i_{s\beta}\right) dt \end{cases} \tag{9}$$

- The estimated torque:

$$T_{m-est} = p.\left(\psi_{s\alpha\text{-est}} i_{s\beta} - \psi_{s\beta\text{-est}} i_{s\alpha}\right) \tag{10}$$

The block diagram of the classical DTC and the diagnostic flowchart diagram are shown in Fig. 2.

1) Hysteresis comparator

The two-level hysteresis comparator in Fig. 3a delimits the flux vector extremity. The comparator, which concerns the couple with three levels of hysteresis shown in Fig. 3b, is designed to control the motor's electromagnetic torque in both senses of rotation by developing a positive or negative torque. Fig. 4c shows a circular ring where the flux vectors are bounded by a band known as the hysteresis band.

Fig. 4 Illustrates the fuzzy logic-based direct torque control structure for an ASM powered via a voltage inverter. A block estimation

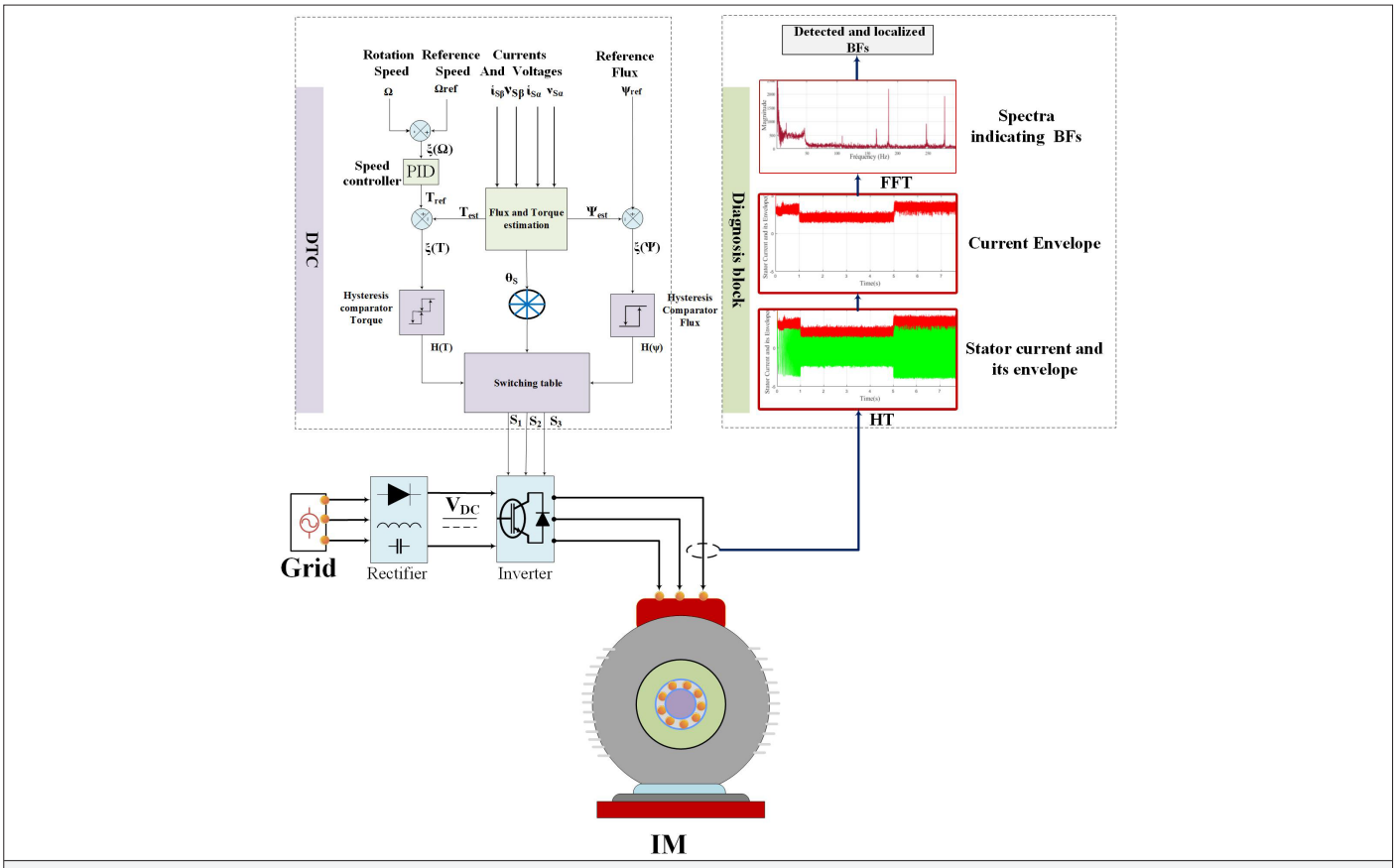

Fig. 2. Direct torque control for ASM and fault diagnosis block.

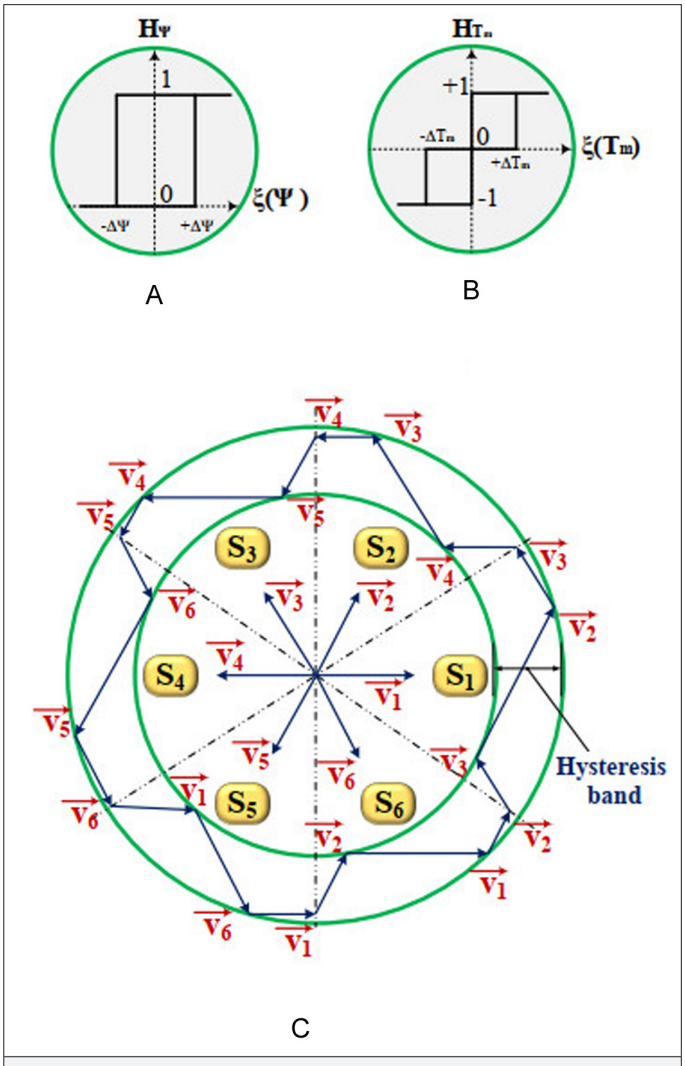

Fig. 3. Hysteresis comparators: (a) Two-level flux. (b) Three-level torque. (c) Flow trajectory.

of the stator torque and flux is done by knowing the imposed voltage vector and the measured stator currents; this estimation is based on the direct calculation method. The rotation speed is compared to its reference, and a Proportional-Integral-Derivative (PID) controller regulates the error to generate the electromagnetic torque reference.

2) Switching table

The voltage vectors are calculated from the sectors and variations of flux and electromagnetic torque, allowing the flux and torque set-points to be followed [11, 12]. Table I, the switching table, shows the procedure for selecting the appropriate voltage vector.

B. Fuzzy logic-based direct torque control

Fuzzy logic, generally known as uncertainty treatment, is considered one of the AI classes [35, 36]. It consists of studying and representing imprecise knowledge and approximate reasoning. It was initially known as a mathematical branch complementary to the theory of classical logic [37, 38].

Currently, FL has found its place in the control field for a wide range of systems, particularly in electrical engineering. It allows the synthesis of controllers that generate efficient control laws without knowing precisely the process to be controlled [39]. This controller type is not based on mathematical expressions but on inferences with different rules using linguistic variables.

The application of FL to direct torque control improves the performance and robustness of the control system. Therefore, a FL controller is used instead of traditional switchboard and hysteresis controllers to improve the system's performance and reduce the electromagnetic flux and torque ripples.

In this system, the inputs to the FL controller are the flux error, the torque error, and the flux angle [35].

- The flux error:

$$\varepsilon_{\psi s} = \psi_{s-ref} - \breve{\psi}_s = \Delta\psi_s \tag{11}$$

- The torque error:

$$\varepsilon_{Tm} = T_{m-ref} - \breve{T}_m = \Delta T_m \tag{12}$$

The variations between a quantity determined using data from the control and the predicted quantity make up these error functions. To improve control while utilizing the fewest possible relations, each input is split into a specific number of fuzzy sets.

Fuzzification, using a rules table to decide the output depending on inputs, and defuzzification are the typical three processes involved in FL [7].

The typical DTC switching table requires that the control rules be set based on the input and output variables. Fig. 5 shows the FL controller's organizational structure.

By establishing membership functions for each input variable, the fuzzification process aims to convert input variables into linguistic variables.

The flux error is shown as the first input variable in Fig. 6a, and its domain of discourse is divided into two fuzzy sets:

(i) The flux error is positive (P); (ii) the flux error is negative (N), and the membership functions used for both fuzzy sets are trapezoidal. The electromagnetic torque error is the second input in Fig. 6b.

Three fuzzy sets comprise its discourse universe: torque error is one of three different values: positive (P), zero (Z), and negative (N). It is decided to use trapezoidal membership functions for the two fuzzy sets (P) and (N).

While the fuzzy set's triangle membership function is selected (Z).

The stator flux position is the third input variable. Fig. 6c depicts the membership functions of the six fuzzy sets (numbered 1–6) that comprise the universe of discourse for this variable.

The selected membership function is triangular for all angles θ_i.

The output variable is separated into two fuzzy sets and three sub-outputs that represent the three switching values (S_1, S_2, and S_3) of the two-level inverter switches (zero and one).

In Fig. 7, the "zero" and "one" states of the output are represented by the blue and yellow horizontal surfaces, respectively.

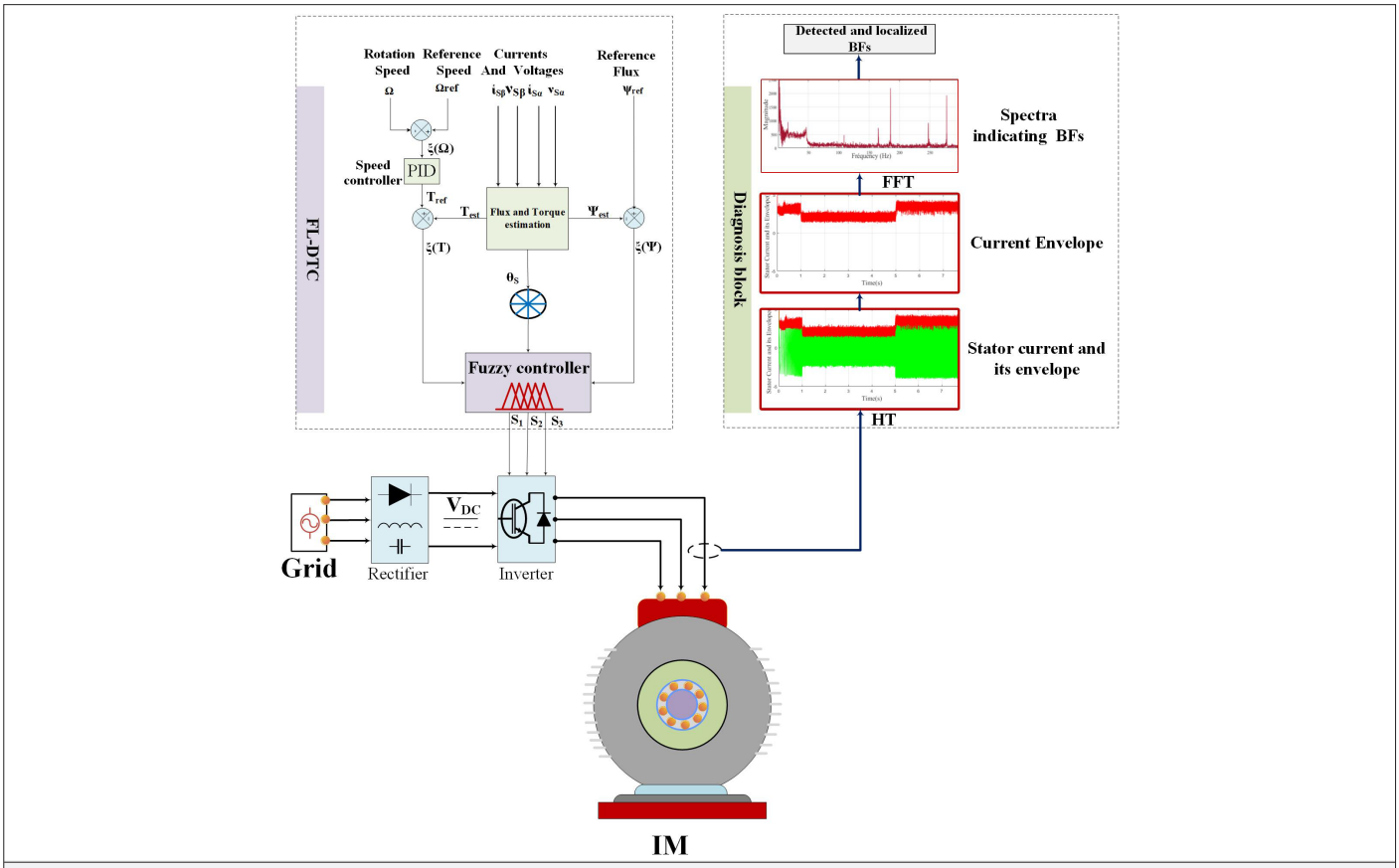

Fig. 4. Block diagram of a FL-DTC control for ASM and the fault diagnosis block

TABLE I. SWITCHING TABLE

		Sectors					
H (Ψ_s)	H (T)	S_1	S_2	S_3	S_4	S_5	S_6
1	1	V_2	V_3	V_4	V_5	V_6	V_1
	0	V_7	V_0	V_7	V_0	V_7	V_0
	-1	V_6	V_1	V_2	V_3	V_4	V_5
0	1	V_3	V_4	V_5	V_6	V_1	V_2
	0	V_0	V_7	V_0	V_7	V_0	V_7
	-1	V_5	V_6	V_1	V_2	V_3	V_4

Table II shows the fuzzy relationships for calculating the controller output variables depending on the input variables:

The control algorithm has 36 relations and uses Mamdani's technique, which is based on the Max–Min decision and has the advantages of being simple to implement and producing good results.

The control rules in terms of input and output variables are expressed as follows:

If (θ is X) and (ε_{Tm} is Y) and (ε_{ψ} is Z) then (V is V_i). Where the fuzzy set of input variables X, Y, and Z, as well as the fuzzy set of output variables, is expressed by V_i (S_1, S_2, S_3).

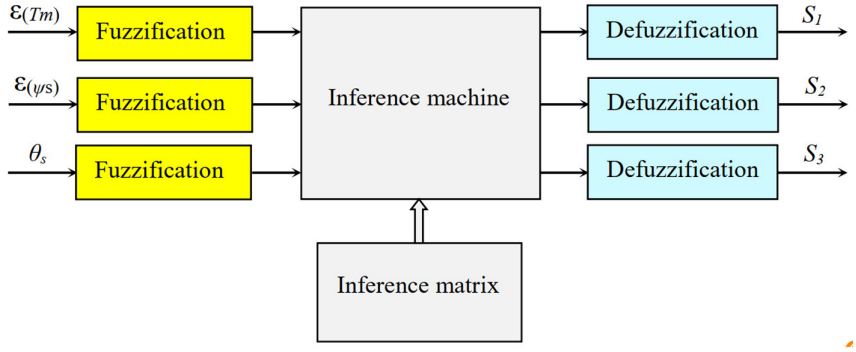

Fig. 5. Illustration of the internal steps of the fuzzy switching table.

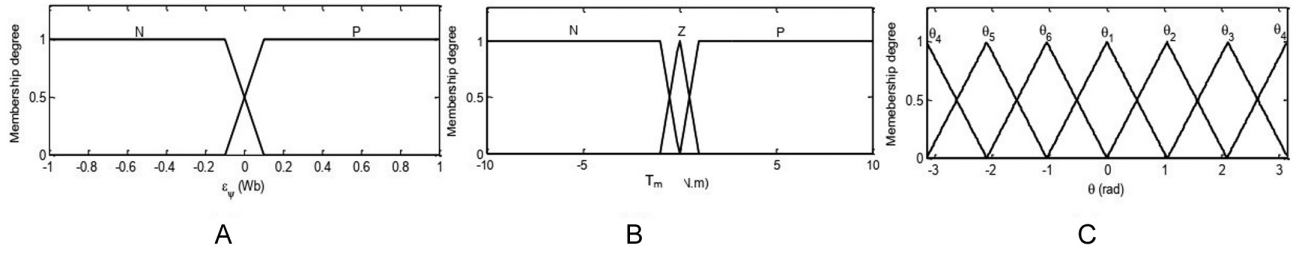

Fig. 6. Membership function of (a) flux linkage error, (b) electromagnetic torque error, and (c) flux position.

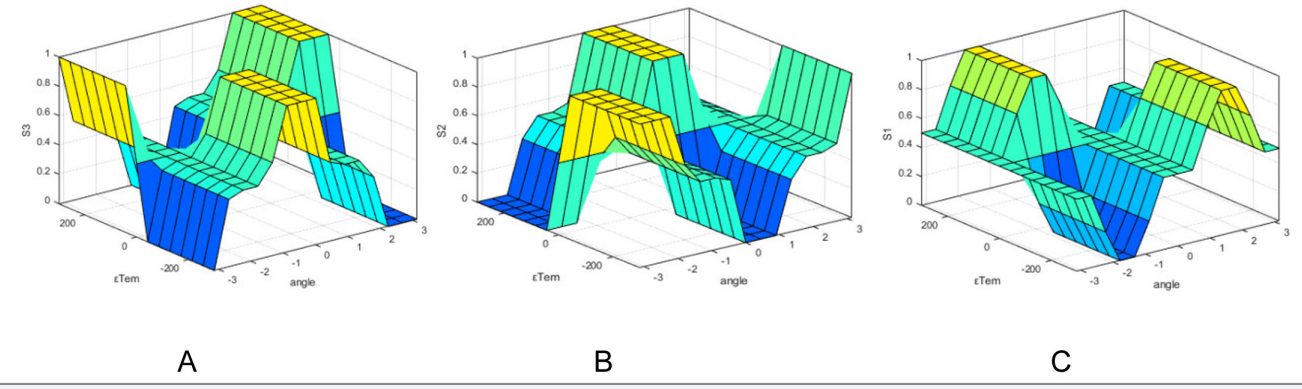

Fig. 7. Membership functions for the output variables: (a) output S1, (b) output S2, and (c) output S3.

TABLE II. SET OF FUZZY RELATIONS

ε_{ψ}	ε_{Tm}	θ_1	θ_2	θ_3	θ_4	θ_5	θ_6
N	N	v_5(001)	v_6(101)	v_1(100)	v_2(110)	v_3(010)	v_4(011)
N	Z	v_0(000)	v_7(111)	v_0(000)	v_7(111)	v_0(000)	v_7(111)
N	P	v_3(010)	v_4(011)	v_5(001)	v_6(101)	v_1(100)	v_2(110)
P	N	v_6(101)	v_1(100)	v_2(110)	v_3(010)	v_4(011)	v_5(001)
P	Z	v_7(111)	v_0(000)	v_7(111)	v_0(000)	v_7(111)	v_0(000)
P	P	v_2(110)	v_3(010)	v_4(011)	v_5 (001)	v_6(101)	v_1(100)

V. HILBERT TRANSFORM

Currently, MCSA remains one of the most important techniques, often used in conjunction with other topologies for detecting faults in ASM. According to ref. [40], there are two main families of diagnostic procedures, model-based methods and the model-free methods. In all of these procedures, MCSA is used at the initial stage.

Fault diagnosis in ASM using model-based techniques requires prior knowledge of the system. It also necessitates an initial hypothesis about the operating conditions to accurately represent the system's performance. The signals generated by mathematical models assist in detecting and identifying faults occurring in the ASM.

Moreover, model-based techniques are primarily dependent on an accurate dynamic model of the system, which equips them to detect unforeseen faults. These approaches leverage "disturbances" or "residuals," which refer to the differences between the outputs of the real physical system and its corresponding mathematical model.

On the other hand, signal-based approaches do not necessarily require a specific model of the system. They rely solely on the signals obtained at key points of interest, typically the input and output terminals. All analyses are conducted either through signal interpretation (by comparing with an ideal case) or via expert systems, which primarily employ pattern recognition techniques. For the sake of simplicity, signal-based approaches are more commonly used today due to their ease of implementation and the fact that most are non-invasive. Fault analysis for ASMs using this approach is conducted in both stationary and transient states.

As mentioned in the introduction, the non-stationarity of the current waveform reduces the fault estimation accuracy when employing FFT-based analysis. That opens the door for the researchers to add other diagnostic methods based on the advanced signal analysis tools in the MCSA framework, such as HT [10, 11, 41].

In addition to offering a high degree of resolution, HT is one of the most advanced signal analysis techniques for machine fault diagnostics [11, 40, 42].

The HT of the actual signal $x(t)$ is the result of the convolution of this signal and the function $1/t$. The mathematical expression of HT is given by [33]:

$$X(t)=\frac{1}{\pi t}*x(t)=\frac{1}{\pi}\int_{-\infty}^{+\infty}\frac{x(t)}{t-\tau}d\tau \tag{13}$$

Since the original signal and its HT are orthogonal, HT is a signal with the same amplitude as the actual signal but with a frequency component that is 90° out of phase with the original signal. As a result, sinusoidal functions become cosinusoidal and vice versa as depicted in Fig. 8 [33, 40].

The HT instantaneous amplitude $a(t)$ and phase $\varphi(t)$ of the HT can be defined as follows [10, 40]:

- The instantaneous amplitude:

$$a(t)=\sqrt{x^2(t)+X^2(t)} \tag{14}$$

- The phase:

$$\varphi(t)=\tan^{-1}\left(\frac{X(t)}{x(t)}\right) \tag{15}$$

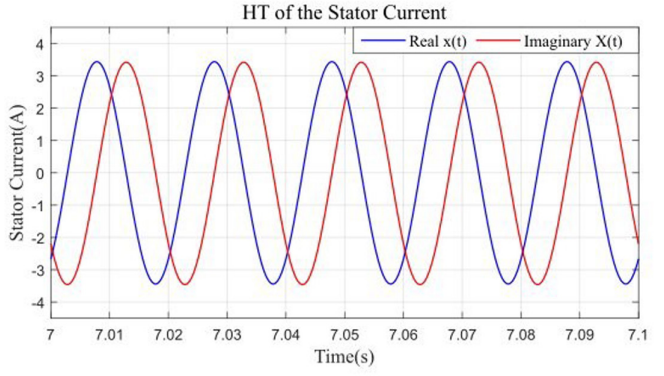

Fig. 8. Hilbert transform of an ASM stator phase current.

The analytical or envelope signal for the HT is shown in Fig. 9.

As a result of the fault within the motor and the lack of a controller, the stator current envelope signal is not distorted and has almost no ripples, as depicted in Fig. 9.

DC components are eliminated from the envelope signal in the frequency domain, while harmonic components are presented; HT in the frequency domain is demonstrated by calculation in refs. [24, 33]. Fig. 10 shows the impact of a fault in the IR of a bearing on the frequency content of the stator current and its envelope. The instantaneous frequencies of the harmonic spectra related to the BFs are given directly by the spectrum of the stator current envelope (SSCE). In contrast, for the current spectrum, these frequencies are related to the supply frequency, and if there is a variation of this supply frequency, as in the case of the use of an inverter, this spectrum of the current becomes useless. This clearly demonstrates HT's interest. In the following part, the simulation results in the frequency domain will be limited to the analysis of the current envelope, by which the instantaneous frequencies will be extracted and interpreted without having recourse to the calculation as a function of the supply frequency.

VI. SIMULATION RESULTS AND DISCUSSIONS

A Simulink model for the ASM has been constructed for healthy and BF conditions with FL-DTC. Two controller approaches, DF and conventional DTC, are explored in order to demonstrate the performance of the suggested system along with the proposed controller. The simulation time chosen is 10 s which is sufficient to show the behavior of the machine while using an appropriate sampling frequency of 10 kHz. The motor used in this study is ASM 1.5 KW, whose parameters are given in Table VI in the appendix. The characteristics for the bearing reference 62052RSC3 are shown in Table VII, while the parameters calculated to identify the characteristic frequencies of BFs are shown in Table VIII. The oscillatory components caused by BFs are simulated by increasing the load torque of the ASM with an amplitude of 2N.m and a frequency of f_c. In all test cases, the ASM is started at no load, then at t = 4 s, a load torque of (T_{ref}=4 N·m), which is 40% of the nominal load torque (T_n=10 N·m) is applied. Initially, the impact of the BFs on the mechanical performance of the ASM in the form of ripples in the electromagnetic torque and rotational speed is investigated. Then, this impact was studied by implementing MCSA based on two points. The first one is the extraction of the SSCE, which indicates the characteristic frequencies of the BFs by the FFT of the

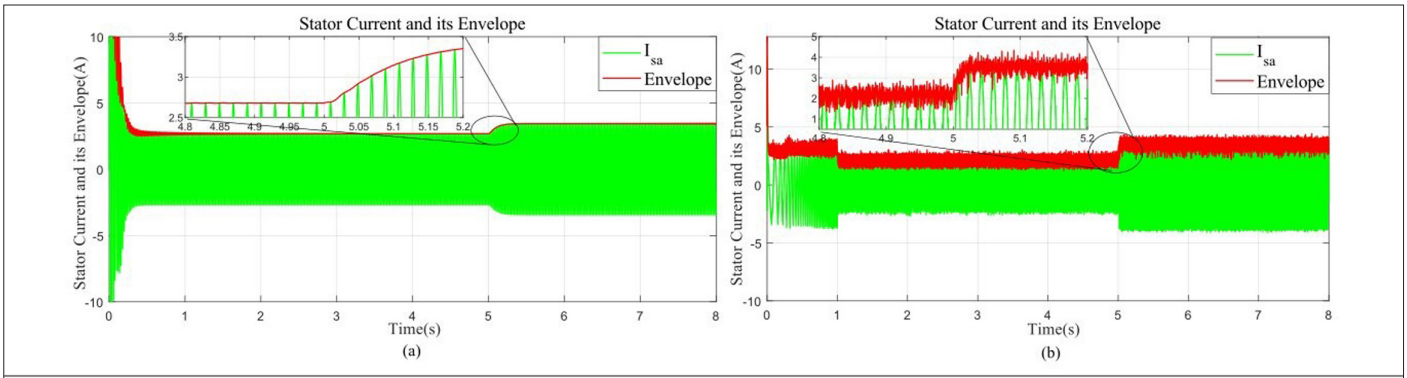

Fig. 9. ASM stator current and its envelope without control (a) and with a direct torque control (b).

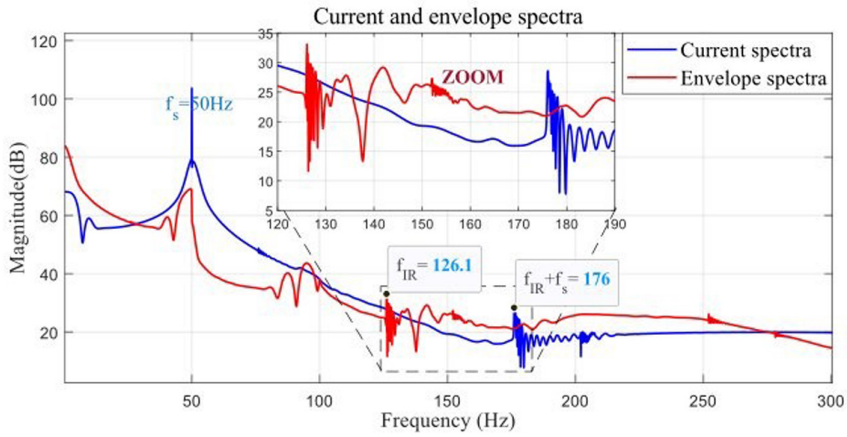

Fig. 10. Spectra of the stator current and its spectrum of the stator current envelope.

stator current envelope. To calculate the effect of the BFs on the stator current, the second step is to determine the THD of the line current.

It is noteworthy to carry out this simulation for an ASM fed by DF before implementing the classical DTC and the intelligent control to show the effect of these control methods on the waveforms.

A. Simulation results for direct flux of the ASM

In this case, the effect of the BF on the mechanical and electrical characteristics will be examined by comparing them to the healthy operation while DF. The profile of the mechanical characteristics (load torque and speed) and electrical characteristics (motor current) are unaffected by the ASM's healthy operation, as shown in Fig. 11. The speed is 1471 rpm at no load and 1375 rpm when the load torque is increased at 4 s as depicted in Fig. 11a. The current, speed, and torque signals are normal and show no ripple, so the THD in this ideal case is zero.

The BFs events in the form of some added ripples impact the mechanical and electrical characteristics. The three BR faults, including IR, OR, and Ball Torque, are simulated in this case. The effects of these three BFs on both mechanical and electrical characteristics will be studied. According to Fig. 12, the ripples in torque and speed are seen for each of the three BFs.

Although the THD is quite little (between 0.03% and 0.09%), the profile of the ASM stator current shown in Fig. 13 illustrates the effect of these BFs on the electrical characteristics in the harmonic spectrum in the SSCE and THD.

From these results, the bearing ball fault generates the largest ripples in both the speed and electromagnetic torque with 0.85 rpm and 0.025 N·m respectively. The speed and torque of the two other BFs faults (IR and OR) have fewer ripples, with their ripple amplitudes not exceeding 0.5 rpm and 0.015 N·m, respectively. In the case of DF, the current THD in the case of BFs depends on the amplitude of the

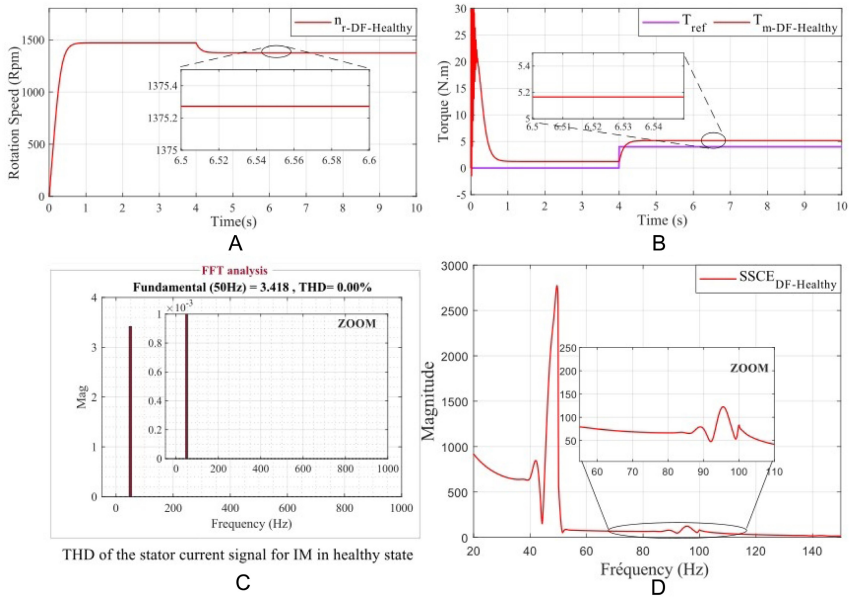

Fig. 11. Mechanical and electrical performances in the healthy state of the ASM with DF: (a) rotation speed, (b) electromagnetic torque, (c) stator current total harmonic distortion, and (d) spectrum of the stator current envelope.

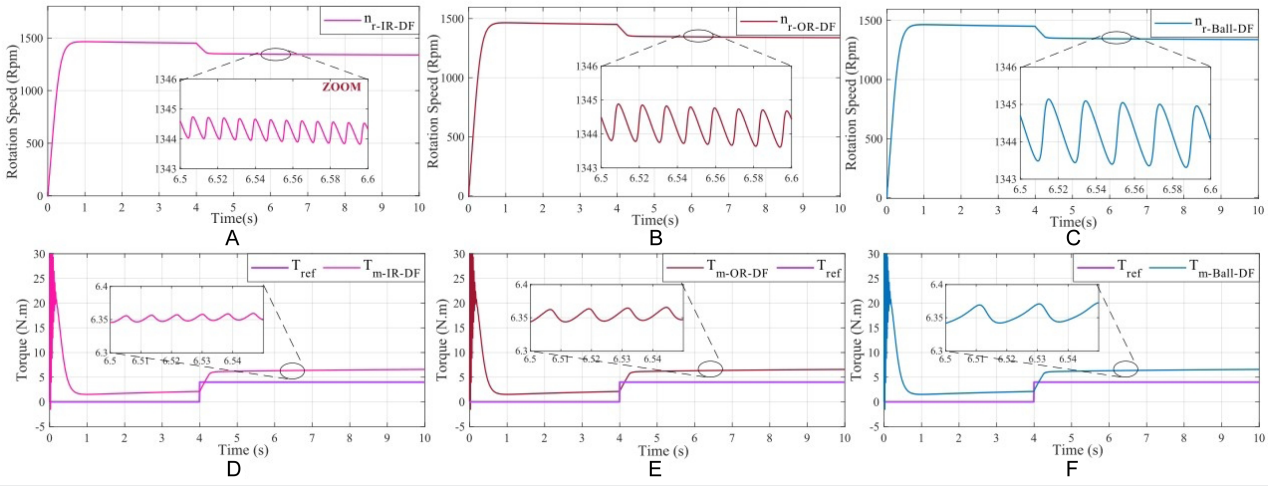

Fig. 12. Mechanical performances in the faulty state of the ASM with direct flux_ rotation speed: (a) inner race, (b) outer race, (c) Ball.Torque: (d) inner race, (e) outer race, and (f) ball.

ripples of the torque and speed magnitudes. As a result, the bearing ball fault causes a higher THD (0.09%), compared with (0.03% and 0.05%, respectively) in the case of the other two BFs (IR and OR).

The rotational frequency and the bearing dimension have the most effects on the characteristic frequencies of BFs, which is confirmed in (3–5). Each BF has two spectra: one at zero load and the other with a load on the left and right side of Fig. 13, respectively. The spectra change positions permanently when the supply voltage or load torque fluctuates, making the diagnostic more challenging and inconclusive.

Fig. 14a–14c shows that in order to determine the severity of the fault, it is crucial to compare the amplitudes related to the BFs to those of the fundamentals. A ratio between the amplitudes of the BFs and the fundamental of SSCE (r_{df}) may be used to assess this comparison as

$$r_{df} = \frac{Mag_{BFs}}{Mag_{fundamental}} \tag{16}$$

The value of r_{df} is 0.01, 0.03, and 0.04, respectively, for the three defects IR, OR, and Ball.

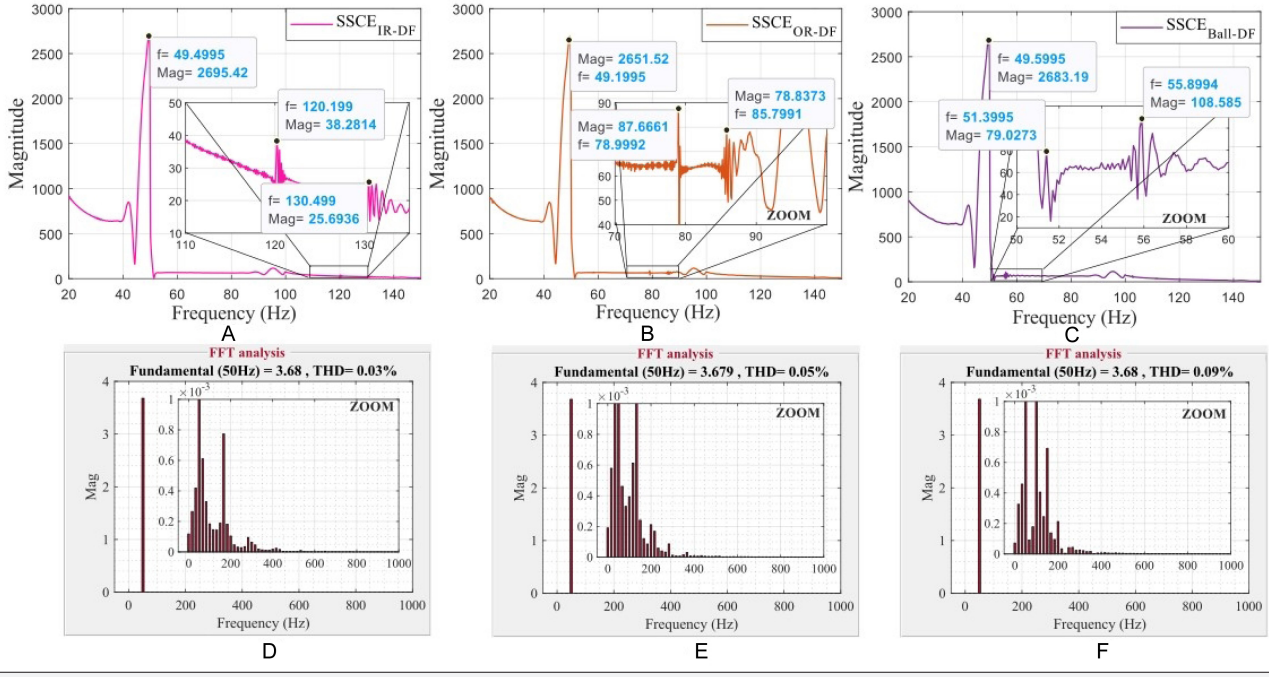

Fig. 13. Electrical performances in the faulty state of the ASM with direct flux_ spectrum of the stator current envelope of the faulty ASM: (a) Inner race. (b) Outer race. (c) Ball. Total hormonic distortion of the stator current: (d) Inner race. (e) Outer race. (f) Ball.

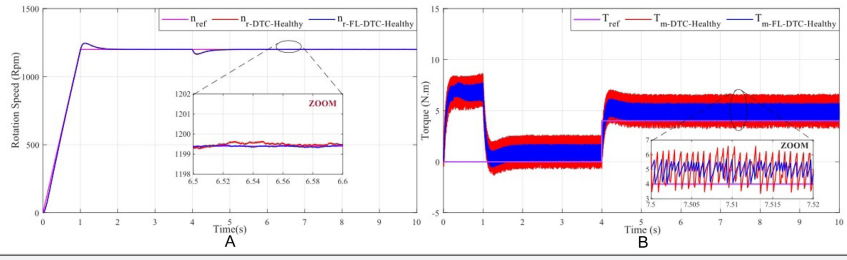

Fig. 14. Mechanical performances of a healthy ASM with direct torque control and fuzzy logic-direct torque control: (a) Speed. (b) Torque.

This showed that the amplitudes of the BF spectra are small in front of the fundamental, particularly in the concrete case where the network includes numerous harmonics, making it difficult to distinguish between different spectra. In the literature, most of the works have recourse to vibratory analysis in the case of mechanical defects because of the MCSA constraints.

The MCSA has difficulties in identifying the BFs when the DF directly provides the ASM with a continual change in speed, and the BFs themselves produce changes in the ASM rotation speed. That calls for the identification of momentaneous frequencies unrelated to the fundamental frequency.

It is also encouraging to note from these results that the severity of the fault is dependent on the bearing defective element and its characteristic frequency. This correlation is shown in Table III.

According to Table VI, the r_{df} is inversely proportional to the characteristic BF's frequency, so this frequency depends mainly on the rotation speed. In the confirmation phase of the presence of BFs, a test at a fixed speed while keeping a reference value should be carried out in order to effectively exhibit the spectra showing their existence by increasing the r_{df} ratio. Then the machine must be isolated from other harmonic sources if the DF is harmonious. Effective and dependable controls can mitigate this drwaback.

First, these controls, which have an inverter, make sure that the ASM and DF are kept apart. Only the inverter's harmonics are present in this case, and the HT utilized in this study allows for their distinction. Also, they permit the desired speed to be maintained, which contributes to the accurate localization of the BFs.

The remaining simulations involve using a FL-DTC to execute the ASM and comparing its performance to that of a traditional DTC to demonstrate its effectivness.

TABLE III. IMPACT OF THE BFS'S FREQUENCY ON THE ELECTRICAL AND MECHANICAL QUANTITIES

BFs	f_c (Hz)	Magnitude of T_m Ripples (N·m)	Magnitude of n_r Ripples (rpm)	THD%	r_{df}
IR	120.2	0.01	0.3	0.03	0.01
OR	79	0.015	0.55	0.05	0.03
Ball	51.4	0.025	0.85	0.09	0.04

THD, total hormonic distortion.

B. Simulation results for the controlled healthy ASM

To display the spectrum produced by BFs, a reference speed of 1200 rpm was used. This speed is consistent for all BF types and their severity. In this case, the bearing's characteristic frequencies are calculed according to (4), (5), and (6):

$$f_{IR} = 108.6Hz; f_{OR} = 71.4Hz; f_{Ball} = 46.4Hz$$

Figs. 14 and 15 show the mechanical and electrical features of the simulation results when DTC and FL-DTC control the ASM. These controls ensure a constant reference speed of 1200 rpm at time $t = 1$ s.

Fig. 14a shows the motor speed profile that is compatible with the reference speed in a healthy state, with some overshoots that cease at 0.5 rpm for DTC and 0.17 rpm for FL-DTC. Additionally, the FL-DTC control results in a torque ripple amplitude of 0.8 N·m compared to 1.7 Nm for the traditional DTC control, demonstrating the influence of the proposed FL-DTC on the mechanical performance of the ASM. The conventional DTC produces large harmonic amplitudes in the frequency range of 150–200 Hz, as depicted in Fig. 15a. When using the FL-DTC, spectral noise is practically eliminated, as seen in Fig. 15b.

The suggested FL-DTC approach is more effective than the DTC method, as shown in Fig. 16a and 16b, where the THD for the current is 15.23% when using DTC and 6.55% when using the proposed FL-DTC method. This intelligent control aids in filtering the signal that has to be analyzed since, in the context of the MCSA's diagnostic, it corresponds to a drop of around 60%.

C. Simulation results for controlled faulty ASM

In this case, the efficacy of the suggested FL-DTC will be assessed, and its performance will be compared to DTC when the machine is working under three different BFs scenarios.

1) Inner race fault of the ASM with direct torque control and fuzzy logic-direct torque control

The IR fault causes some in the speed, torque, and current profiles, as depicted in Figs. 18–20. When compared to the DTC, as shown in Fig. 17a and 17b, the suggested FL-DTC was successful in tracking the reference speed and the reference torque with reduced ripples. According to Figs. 18 and 19, employing FC-DTC and DTC, respectively, the THD decreased to 6.31% compared to 15.2%.

2) Outer race fault of the ASM with direct torque control and fuzzy logic-direct torque control

The proposed FL-DTC succeeded in tracking both the reference speed and the reference torque with fewer ripples when compared to the DTC as depicted in Fig. 20; also, the FL-DTC control

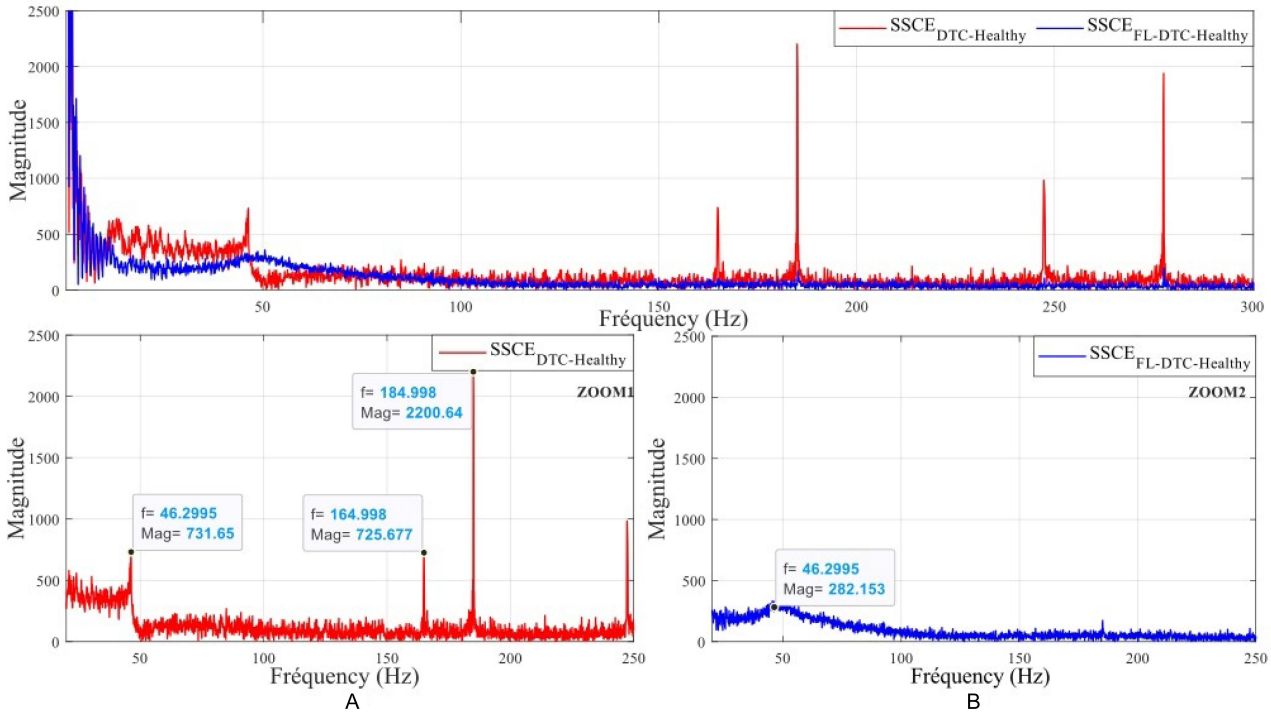

Fig. 15. Spectrum of the stator current envelope of a healthy ASM.

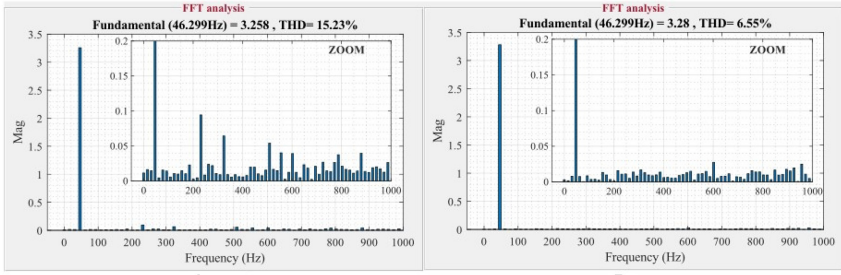

Fig. 16. THD of the stator current of a healthy ASM with _ (a) direct torque control and (b) fuzzy logic-direct torque control.

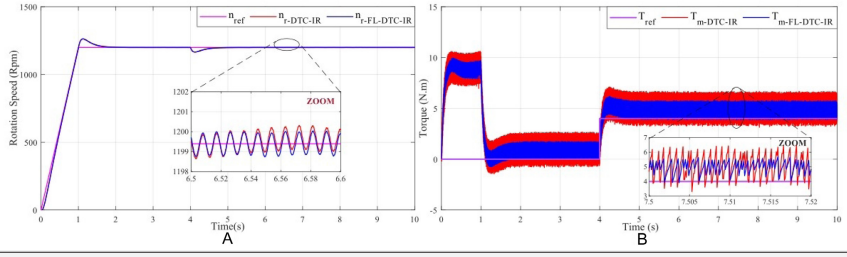

Fig. 17. Mechanical performances with IR fault of the ASM with direct torque control and fuzzy logic-direct torque control: (a) Speed. (b) Torque.

decreases this THD to 6.55% compared to 15.37% as illustrated in Figs. 21 and 22.

3) Ball bearing fault of the ASM with direct torque control and fuzzy logic-direct torque control

The proposed FL-DTC succeeded in tracking both reference speed and torque with less ripple than the DTC, as shown in Fig. 23. In addition, FL-DTC reduced THD to 6.88% compared to 15.03%, as shown in Figs. 24 and 25.

D. Discussion Summary

1) Mechanical performances

According to Figs. 17, 20, and 23, BFs cause amplitude ripples in the speed signature of about 1.5 rpm when the ASM is controlled

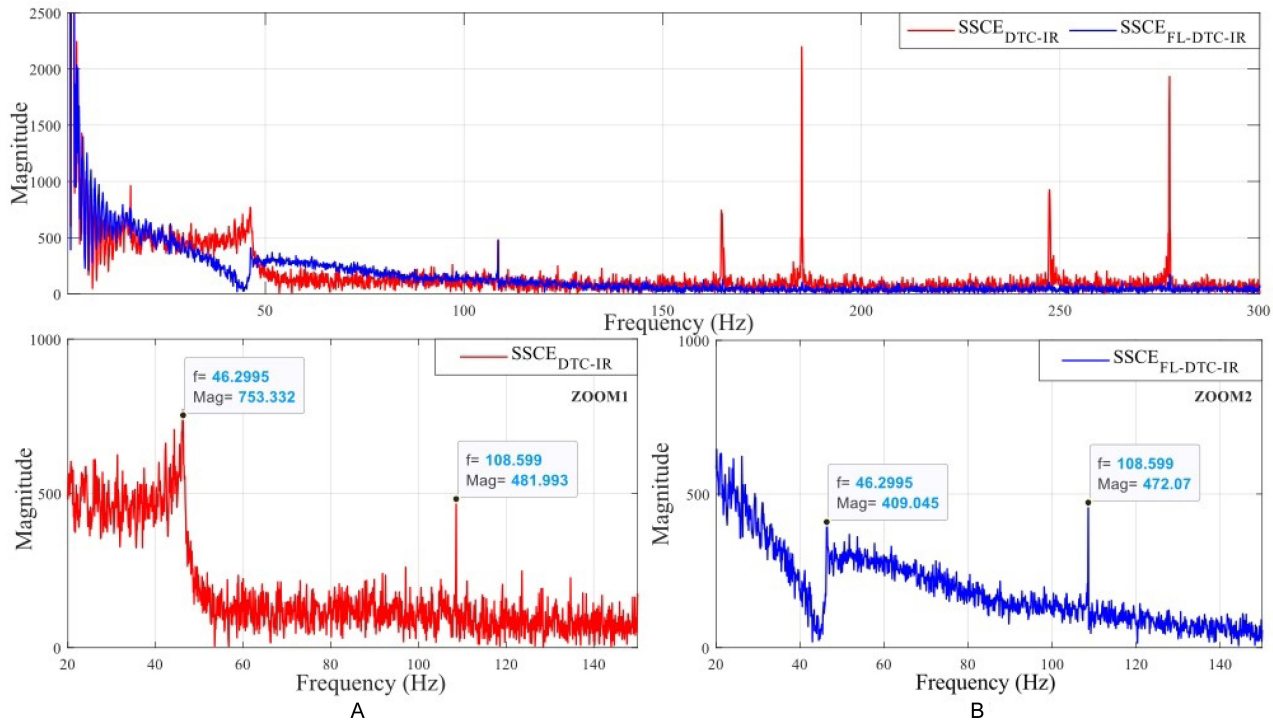

Fig. 18. Spectrum of the stator current envelope with IR fault in the ASM (Top) with (a) zoom of SSEDTC-IR and (b) zoom of SSE FL-DTC-IR.

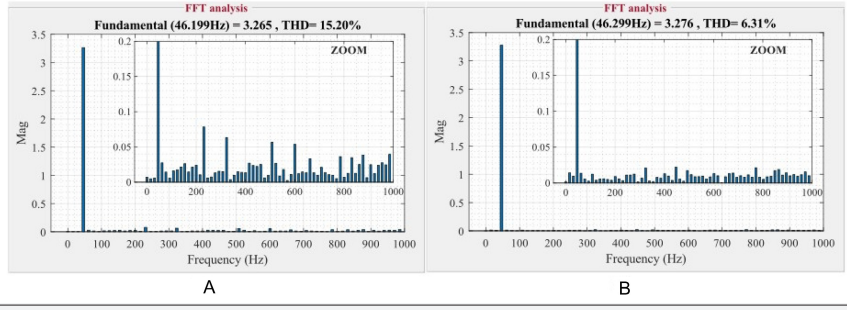

Fig. 19. THD of the stator current with IR fault in the ASM with (a) direct torque control and (b) fuzzy logic-direct torque control.

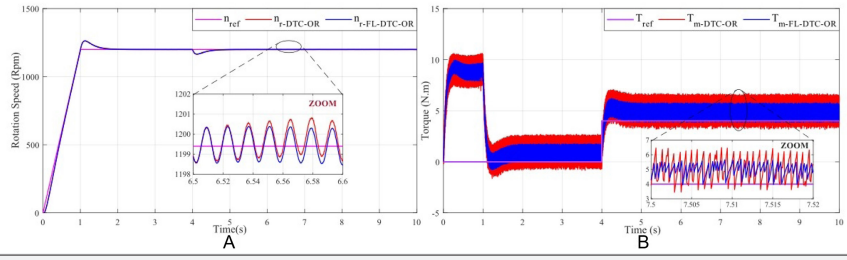

Fig. 20. Mechanical performances with outer race fault of the ASM with direct torque control and fuzzy logic-direct torque control: (a) Speed. (b) Torque.

by conventional DTC, and amplitude ripples in the electromagnetic torque exceed 1.75 N·m when FL-DTC controls the ASM. These values become 1.3 rpm and 0.85 N·m for speed and torque, respectively, when FL-DTC controls the motor.

2) Electrical performances

In this diagnostic context, the primary performance of the FL-DTC control is the distinction of spectra related to BFs, rendering them more precise than those caused by the control (Figs. 15, 18, 21, and

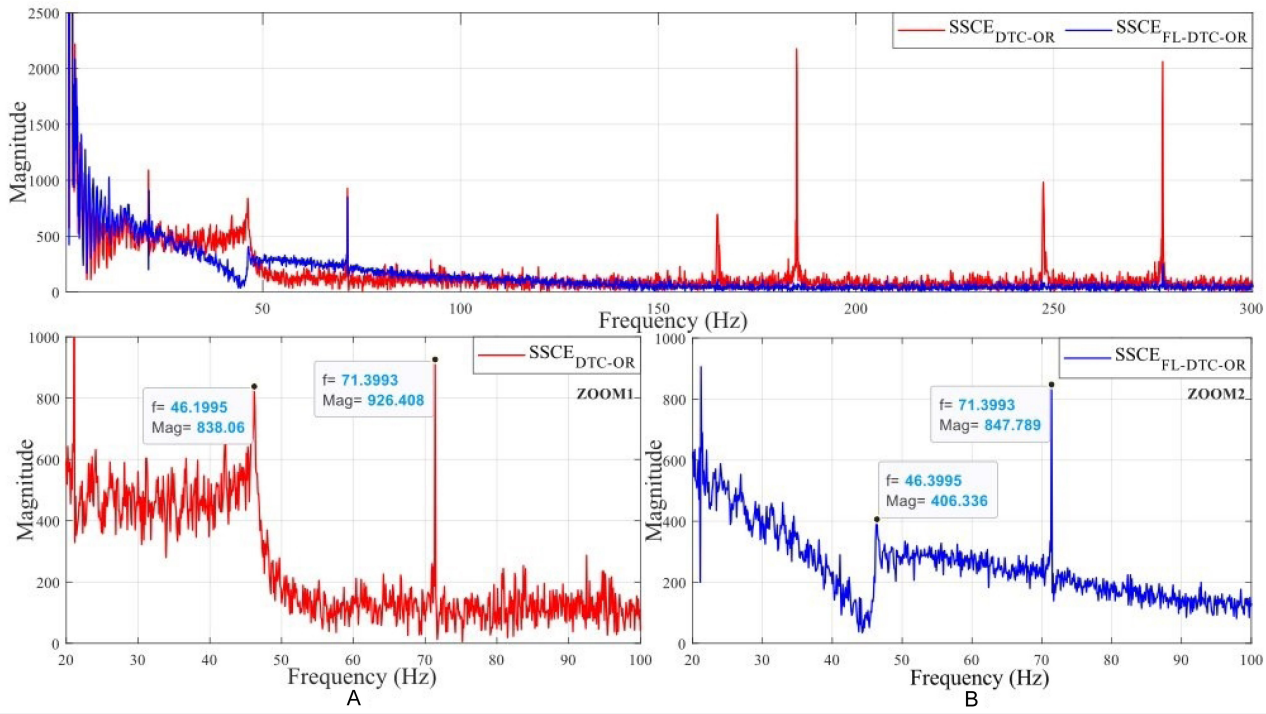

Fig. 21. Spectrum of the stator current envelope with outer race fault in the ASM.

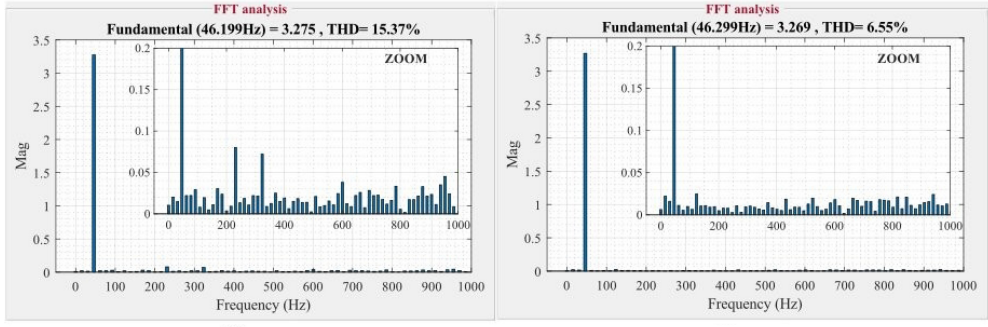

Fig. 22. Total hormonic distortion of the stator current with outer race fault in the ASM with (a) direct torque control and (b) fuzzy logic-direct torque control.

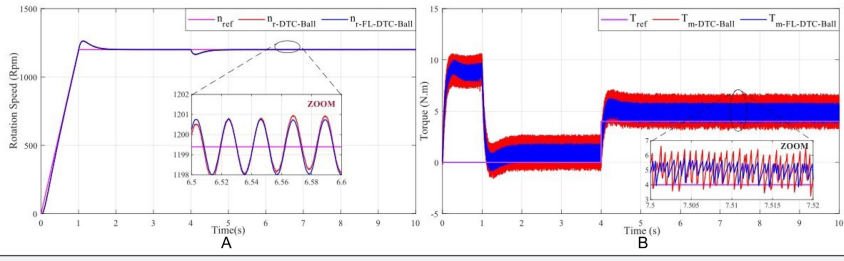

Fig. 23. Mechanical performances with Ball bearing fault of the ASM with direct torque control and fuzzy logic-direct torque control: (a) Speed. (b) Torque.

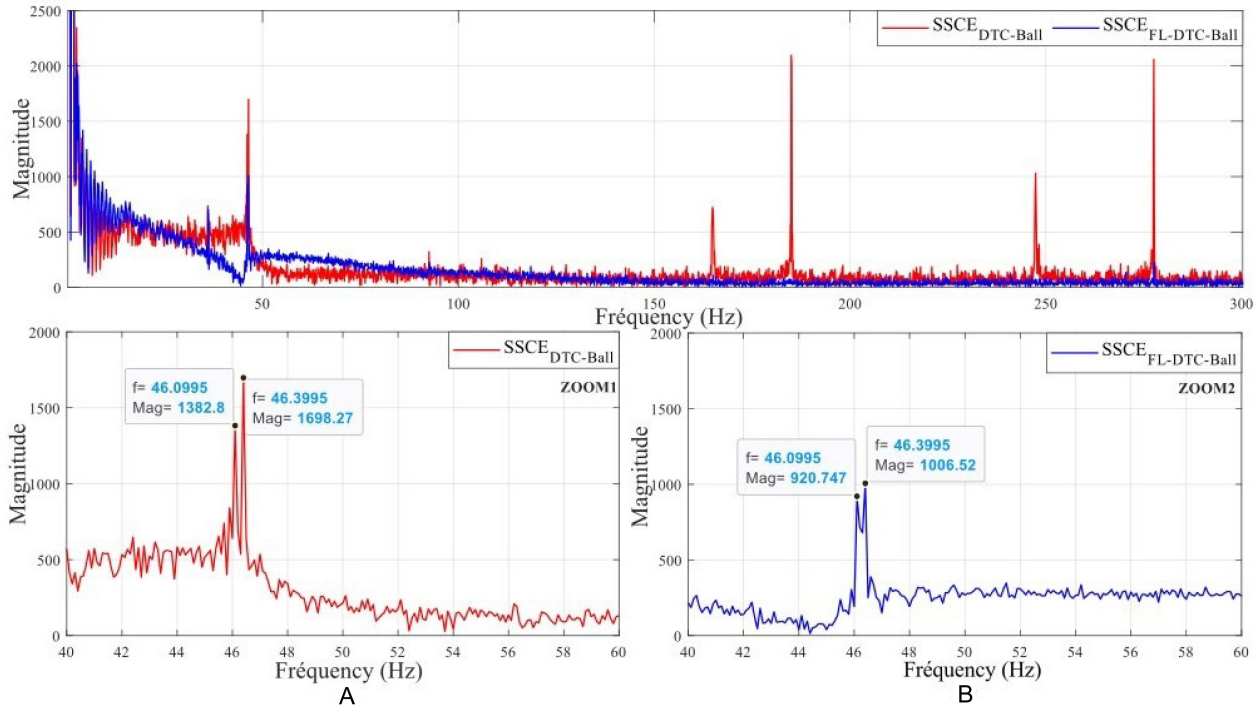

Fig. 24. Spectrum of the stator current envelope with Ball bearing fault in the ASM.

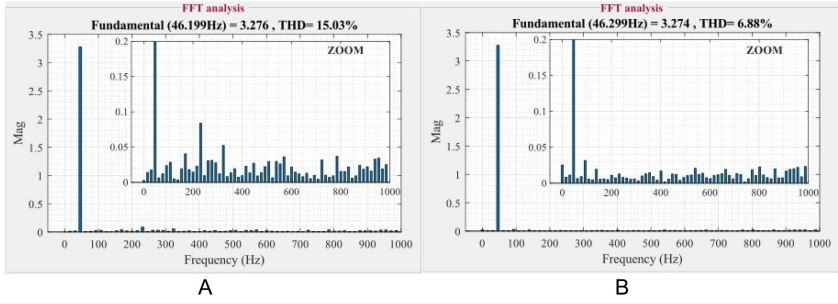

Fig. 25. THD of the stator current with Ball bearing fault in the ASM with (a) direct torque control and (b) fuzzy logic-direct torque control.

24); the ratio r_{df} measures this performance. In fact, even if these spectra are clearly distinguished, the use of FL-DTC makes them more evident by reducing spectral noise caused by the control and increasing the amplitudes of the dependent spectra of BFs, as shown in Fig. 22 for the OR fault, where this ratio r_{df} is 1.10 in the case of classical DTC and 2.08 in the case of FL-DTC.

Moreover, in Figs. 19, 22 and 25, which show the THD of the current in the case of BFs, the values of this rate for the conventional DTC arrive at 15.37% and 6.88% for the FL-DTC; this proves that for diagnostic purposes, the THD is not conclusive in the presence of the controls, as these values are very close for the three BFs (IR, OR, and Ball). Also, the harmonics proportion caused by the BFs is significantly inferior to those caused by the two controls (0.09% in the DF case, 15.37% in the DTC case, and 6.88% in the FL-DTC case).

The summary of the performance of FL-DTC and DTC during the three BFs is summarized in Table IV.

The benefits of the chosen approach are shown in Table VI, where it is highly evident how the FL-DTC control affects the mechanical performance of speed and electromagnetic torque in a healthy condition. In fact, the speed fluctuations are nearly zero (0.17 Rpm) compared to 0.5 Rpm when traditional DTC is used, significantly reducing torque ripples (0.8 N·m for FL-DTC vs. 1.7 N·m for classic DTC).

The FL-DTC control limits the amplitudes of the torque and speed variations to 0.85 N·m and 1.3 rpm successively in the case of BFs in the bearing ball, as compared to 1.75 N·m and 1.5 rpm in the case of traditional DTC, i.e. a reduction of 13% in the amplitudes of the speed variations compared to the traditional DTC control, which is 0.025 N·m and 0.85 rpm in the case of DF, i.e. a reduction in the amplitudes of speed variation of 13% compared to the traditional DTC control. In the cases of the IR and OR faults, the amplitudes of speed variations are reduced by 25% and 23.5%, respectively, when compared to traditional DTC. Similarly, the amplitudes of the torque ripples in the presence of these three BFs (IR, OR, and Ball) are decreased by

TABLE IV. COMPARISON OF THE PERFORMANCE IN A HEALTHY STATE AND IN THE PRESENCE OF BEARING FAULTS.

Variable Analyzed	Control Technique	Control	Performances	Etat Sain	IR BF	OR BF	Ball BF
Current	Open loop	DF	r_{df}	0	0.01	0.03	0.04
	Closed loop	DTC		0	0.64	1.1	1.20
	Closed loop	FL-DTC		0	1.15	2.08	1.1
Current	Open loop	DF	THD (%)	0	0.03	0.05	0.09
	Closed loop	DTC		15.23	15.20	15.37	15.03
	Closed loop	FL-DTC		6.55	6.31	6.55	6.88
Torque	Open loop	DF	Torque ripples (N·m)	0	0.01	0.015	0.025
	Closed loop	DTC		1.7	1.6	1.6	1.75
	Closed loop	FL-DTC		0.8	0.62	0.75	0.85
Speed	Open loop	DF	Overshoot (rpm)	0	0.3	0.5	0.85
	Closed loop	DTC		0.5	0.8	0.85	1.5
	Closed loop	FL-DTC		0.17	0.6	0.65	1.3

BF, bearing faults; DF, direct fed; DTC, direct torque control; FL-DTC, fuzzy logic-direct torque control; IR, inner race; OR, outer race; THD, total harmonic distortion.

61.25%, 53.12%, and 51.42%, respectively, with FL-DTC compared to conventional DTC.

Furthermore, in the case of DF, the THD values clearly show the impact of each BF on the stator current; however, in the presence of both controls, these values do not give any useful information about the faults in the ASM.

The values of the r_{df} ratio are the most essential parameter because they illustrate the advantage of FL-DTC in distinguishing the spectra indicating BFs, especially for the two BFs, IR and OR (0.64 for the classical DTC against 1.15 for the FL-DTC). Also, for the Ball fault, whose characteristic frequency is very close to the voltage frequency at the output of the inverter, this ratio is almost the same (1.2 for the classical DTC against 1.1 for the FL-DTC) Indeed, for the results to be conclusive, it is better to choose reference speeds that result in characteristic frequencies sufficiently higher than the fundamental frequency.

3) Comparison with some recent studies

In this section, the Table V shows a brief comparison is made with other recent works which take into account the control in the context of fault diagnosis in ASMs. the criteria for this comparison concern the type of fault, the control, the signal processing method adopted

TABLE V. COMPARISON WITH SOME OTHERS RECENT STUDIES

Studies	ASM Fault	Control	Variable	Method	Control (Contributor or Disturber)
[2]	BRB	DTC	Current	DWT	Disturber
[3]	BRB	IFOC	Current	ANN and HT	Disturber
[4]	BRB	FOC	Current	DWT	Disturber
[5]	BRB	FOC	Current	FFT	Disturber
[12]	Short-circuit	Frequency converter	Vibration	CWT and CNN	Disturber
[40]	BFs	ANN-DTC	Current	HT and FFT	Contributor
[43]	Short-circuit	IFOC	Current, torque, and speed	RMS, Average,...	Disturber
[44]	BRB—short-circuit	Frequency converter	vibration	ANNs	Disturber
[45]	BRB—short-circuit	IFOC	Torque	DWT and ANN	Disturber
This study	BFs	FL-DTC	Stator current	HT and FFT	Contributor

ANN, artificial neural networks; BF, bearing faults; BRB, broken rotor bar; DTC, direct torque control; DWT, discrete wavelet transform; FFT, fast fourier transform; FL-DTC, fuzzy logic-direct torque control; HT, Hilbert transform; IFOC, indirect field oriented control. CWT, continuous wavelet transform; CNN, convolutional neural network; FOC, field-oriented control.

TABLE VI. THE ASYNCHRONOUS MACHINE PARAMETERS

Parameter	Value
Nominal power	P_n = 1.5 kW
Mutual inductance maximum	L_m= 0.082 H
Self-inductance	L_s= 0.36 H;
Rotor inductance	L_r=0.02143 H
Stator resistor	R_s= 4Ω
Rotor resistor	R_r= 0.8Ω
Total inertia	J=0. 024 Kg.m^2
Pair pole number	p=2
Viscous frictions	f= 0.004 045 Kg.m^2/s

TABLE VII. BEARING SPECIFIC DIMENSIONS

Bearing Reference	Outer Diameter	Inner Diameter	Angle of Contact α	Width	Balls Number
62052RSC3	52 mm	25 mm	0	15 mm	9

TABLE VIII. VALUES DETERMINED BY CALCULATION

Ball diameter	Average Cage Diameter	Balls Number	Cosα
7.94 mm	38.5 mm	9	1

and whether the control represents a contributing or disturbing element for fault diagnosis in this type of machine.

This comparison, presented in Table VI, shows that the majority of studies in the literature that consider control focus on BRBs faults and treat the control as a disturbing element, which leads them to adopt advanced signal processing and/or intelligent methods. The authors in ref. [40] addresses BFs and utilizes the ANN-DTC control to aid in the diagnosis. In ref. [46], another recent study presents a comparison between ANN-DTC and FL-DTC in terms of their contribution to the diagnosis of BFs.

VII. CONCLUSION

This research employs a method of diagnosing BFs based on MCSA, which was partnered with a HT and an intelligent speed control FL-DTC. The purpose of this research is to design a control that is efficient and has the least amount of THD, as well as maintain the rotational speed at a specific reference value; this will allow the analysis of the stator's current envelope in the domain to be employed to extract the instantaneous frequencies and to differentiate the spectrum of BFs from the others, this will increase the effectiveness of diagnostics in ASMs that are controlled by closed-loop systems.

First, the parts that oscillate in the BFs were recreated. The FL-DTC protocol is then employed to control the ASM. Subsequently, a time frequency domain analysis of the current profile was conducted. The results of the simulation using MATLAB/Simulink, as well as their understanding, are listed below:

1. The diagnosis of LFs is accurate thanks to the control of the speed of the ASM by the FL-DTC and the reduction in THD compared with conventional DTC of more than 50%, in all cases.
2. The FL-DTC method reduces the amplitude of the harmonic spectrum produced by the control, and better distinguishes harmonics from BFs. The values of the r_{df} ratio illustrate the advantage of FL-DTC in distinguishing the spectra indicating BFs, especially for the two BFs, IR and OR (0.64 for the classical DTC against 1.15 for the FL-DTC).
3. Because it is less sensitive to alterations in load rotation, envelope current analysis using HT and FFT is very useful for recognising mechanical faults. In this way, the specific frequencies in the spectrum that indicate faults (f_{IR}, f_{OR}, f_{ball}) are easily recognizable and are not linked to the supply frequency, making it easier to identify BFs.

Future research could develop this work to test it experimentally in the presence of various electrical faults such as BRBs and mechanical faults such as BFs. Also, the processing of ASM current and noise data instead of signal processing would be interesting and would make it possible to carry out intelligent classification of the various faults in rotating machines.

Availability of Data and Materials: The data that support the findings of this study are available on request from the corresponding author.

Peer-review: Externally peer-reviewed.

Author Contributions: Concept – A.D., S.M., N.E.O.; Supervision – A.E.I., A.D., S.M., N.E.O., A.C., M.M.; Resource – A.E.I., A.D., S.M., N.E.O., A.C., M.M.; Materials – A.E.I., A.D., S.M., N.E.O., A.C., M.M.; Data Collection and/or Processing – A.E.I., A.D., S.M., N.E.O., A.C., M.M.; Analysis and/or Interpretation – A.EL., A.C., M.M.; Search – A.E.I., A.D., S.M., N.E.O., Writing – A.E.I., S.M., N.E.O., Critical Review – A.E.I., A.D., S.M., N.E.O., A.C., M.M.

Declaration of Interests: The authors have no conflict of interest to declare.

Funding: The authors declare that this study has received no financial support.

REFERENCES

1. F. Asghar, M. Talha, and S. H. Kim, "Neural network based fault detection and diagnosis system for three-phase inverter in variable speed drive with induction motor," *J. Control Sci. Eng.*, vol. 2016, pp. 1–12, 2016. [CrossRef]
2. R. Senthil Kumar, and I. G. Christopher Raj, "Broken rotor bar fault detection using DWT and energy eigenvalue for DTC fed induction motor drive," *Int. J. Electron.*, vol. 108, no. 8, pp. 1401–1425, 2021. [CrossRef]
3. R. Senthil Kumar et al., "A combined HT and ANN based early broken bar fault diagnosis approach for IFOC fed induction motor drive," *Alex. Eng. J.*, vol. 66, pp. 15–30, 2023. [CrossRef]
4. T. Ameid, A. Menacer, H. Talhaoui, and Y. Azzoug, "Discrete wavelet transform and energy eigen value for rotor bars fault detection in variable speed field-oriented control of induction motor drive," *ISA Trans.*, vol. 79, pp. 217–231, 2018. [CrossRef]
5. T. Ameid, A. Menacer, H. Talhaoui, and I. Harzelli, "Broken rotor bar fault diagnosis using fast Fourier transform applied to field-oriented control induction machine: Simulation and experimental study," *Int. J. Adv. Manuf. Technol.*, vol. 92, no. 1–4, pp. 917–928, 2017. [CrossRef]
6. M. Defdaf, F. Berrabah, A. Chebabhi, and B. D. E. Cherif, "A new transform discrete wavelet technique based on artificial neural network for induction motor broken rotor bar faults diagnosis," *Int. Trans. Electr. Energy Syst.*, vol. 31, no. 4, 2021. [CrossRef]
7. Y. Yu, Y. Zhao, B. Wang, X. Huang, and D. Xu, "Current sensor fault diagnosis and tolerant control for VSI-based induction motor drives," *IEEE Trans. Power Electron.*, vol. 33, no. 5, pp. 4238–4248, 2018. [CrossRef]
8. R. V. Banin, V. A. Butorin, and I. B. Tsarev, "Studying rate of changing parameters of bearings' technical condition in asynchronous motors for

agricultural purpose when transmitting torque by mechanical clutch," in *Proceedings of the 6th International Conference on Industrial Engineering (ICIE 2020)*, A. A. Radionov, and V. R. Gasiyarov, Ed. Cham: Springer International Publishing, 2021, pp. 1206–1213. [CrossRef]
9. P. Gangsar, and R. Tiwari, "Signal based condition monitoring techniques for fault detection and diagnosis of induction motors: A state-of-the-art review," *Mech. Syst. Signal Process.*, vol. 144. 2020. [CrossRef]
10. I. Takahashi, and Y. Ohmori, "High-performance direct torque control of an induction motor," *IEEE Trans. Ind. Appl.*, vol. 25, no. 2, pp. 257–264, 1989. [CrossRef]
11. W. Laala, A. Guedidi, and A. Guettaf, "Bearing faults classification based on wavelet transform and artificial neural network," *Int. J. Syst. Assur. Eng. Manag.*, vol. 14, No. 1, pp. 37–44, 2023. [CrossRef]
12. T. ZAS, "Mnickas", J. Vanagas, *K. Dambrauskas, and A. Kalvaitis*, "A technique for frequency converter-fed asynchronous motor vibration monitoring and fault classification, applying continuous wavelet transform and convolutional neural networks, *Energies*, vol. 13, no. 14, 2020. [CrossRef]
13. A. Pilloni, A. Pisano, M. Riera-Guasp, R. Puche-Panadero, and M. Pineda-Sanchez, *Fault Detection in Induction Motors*, 2013.
14. M. Blödt, P. Granjon, B. Raison, G. Rostaing, and R. Gilles, "Models for bearing damage detection in induction motors using stator current monitoring," *Electron. Eng.* Institut Electr, vol. 55, no. 4, p. 1813–1822, 2008. [CrossRef]
15. H. Esen, M. Inalli, A. Sengur, and M. Esen, "Forecasting of a ground-coupled heat pump performance using neural networks with statistical data weighting pre-processing," *Int. J. Therm. Sci.*, vol. 47, no. 4, pp. 431–441, 2008. [CrossRef]
16. P. M. Özturan, A. Bozanta, B. Basarir-Ozel, E. Akar, and M. Coşkun, "A roadmap for an integrated university information system based on connectivity issues: Case of Turkey," *Int. J. Manag, Sci. Inf. Technol.*, vol. 17, no. 17, pp. 1–23, 2015. [CrossRef]
17. M. B. Abd-El-Malek, A. K. Abdelsalam, and O. E. Hassan, "Novel approach using Hilbert Transform for multiple broken rotor bars fault location detection for three phase induction motor," *ISA Trans.*, vol. 80, pp. 439–457, 2018. [CrossRef]
18. A. Bouras, S. Bennedjai, and S. Bouras, "ExperASMental detection of defects in variable speed fan bearing using stator current monitoring," *SN Appl. Sci.*, vol. 2, no. 5, 2020. [CrossRef]
19. G. H. Bazan, A. Goedtel, O. Duque-Perez, and D. Morinigo-Sotelo, "'Multi-fault diagnosis in three-phase induction motors using data optASMization and machine learning techniques,' *Electron.*," *Electronics*, vol. 10, no. 12, 2021. [CrossRef]
20. R. Senthil Kumar *et al.*, "A method for broken bar fault diagnosis in three phase induction motor drive system using Artificial Neural Networks," *Int. J. Ambient Energy*, vol. 43, no. 1, pp. 5138–5144, 2022. [CrossRef]
21. M. Feldman, "Hilbert transform in vibration analysis," *Mech. Syst. Signal Process.* Cambridge, United States of America: Academic Press, vol. 25, no. 3, pp. 735–802, 2011. [CrossRef]
22. S. K. Gundewar, and P. V. Kane, "Condition monitoring and fault diagnosis of induction motor," *J. Vib. Eng. Technol.* Berlin: Springer, vol. 9, no. 4, pp. 643–674, 2021. [CrossRef]
23. R. Puche-Panadero, J. Martinez-Roman, A. Sapena-Bano, J. Burriel-Valencia, and M. Riera-Guasp, "Fault diagnosis in the slip–frequency plane of induction machines working in tASMe-varying conditions," *Sensors (Switzerland)*, vol. 20, no. 12, pp. 1–25, 2020. [CrossRef]
24. S. Drid, M. S. Nait-Said, and M. Tadjine, "Double flux oriented control for the doubly fed induction motor," *Electr. Power Compon. Syst.*, vol. 33, no. 10, pp. 1081–1095, 2005. [CrossRef]
25. P. Konar, and P. Chattopadhyay, "Multi-class fault diagnosis of induction motor using Hilbert and Wavelet Transform," *Appl. Soft Comput.*, vol. 30, pp. 341–352, 2015. [CrossRef]
26. M. Depenbrock, "Direct self-control (DSC) of inverter fed Induktion machine," IEEE Power Electron. Spec. Conf., 1987, pp. 632–641. [CrossRef]
27. M. Tabasi, M. Mostafavi, et M. Ojaghi, "Motor current signature analysis for detecting local defects on rolling-element bearings of induction motors," *Arab. J. Sci. Eng.*, vol. 48, no. 11, pp. 14811–14822, 2023. [CrossRef]
28. M. O. Mustafa, D. Varagnolo, G. Nikolakopoulos, and T. Gustafsson, "Detecting broken rotor bars in induction motors with model-based support vector classifiers," *Control Eng. Pract.*, vol. 52, pp. 15–23, 2016. [CrossRef]
29. D. Ahmed, B. Mokhtar, and B. Aek, "DTC-ANN-2-level hybrid by neuronal hysteresis with mechanical sensorless induction motor drive using Kubota observer," *IJPEDS*, vol. 11, no. 1, pp. 34–44, 2020. [CrossRef]
30. H. Benbouhenni, *Seven-Level Direct Torque Control of Induction Motor Based on Artificial Neural Networks with Regulation Speed Using Fuzzy PI Controller*, 2018.
31. J. Zhang, S. Li, and Z. Xiang, "Adaptive fuzzy finite-time fault-tolerant control for switched nonlinear large-scale systems with actuator and sensor faults," *J. Franklin Inst.*, vol. 357, no. 16, pp. 11629–11644, 2020. [CrossRef]
32. R. N. Toma, and J. M. KASM, "Article bearing fault classification of induction motors using discrete wavelet transform and ensemble machine learning algorithms," *Appl. Sci.*, vol. 10, no. 15, 2020. [CrossRef]
33. H. Benli, "Performance prediction between horizontal and vertical source heat pump systems for greenhouse heating with the use of artificial neural networks," *Heat Mass Transfer*, vol. 52, no. 8, pp. 1707–1724, 2016. [CrossRef]
34. H. Mohammed, and A. Meroufel, "Contribution to the Neural network speed estASMator for sensor-less fuzzy direct control of torque application using double stars induction machine," *Int. Conf. Electr. Sci. Technol. Maghreb. Cist.* vol. 5, no. 4, 2014. [CrossRef]
35. S. Ahamad, M. Mohseni, V. Shekher, G. F. Smaisim, A. Tripathi, and J. Alanya-Beltran, "A Detailed Analysis of the Critical Role of artificial intelligence in Enabling High-Performance Cloud Computing Systems" 2nd International Conference on Advance Computing and Innovative Technologies in Engineering (ICACITE), 2022, pp. 156–159. [CrossRef]
36. A. Alizadeh *et al.*, "Evaluation of the effects of the presence of ZnO -TiO2 (50 %–50 %) on the thermal conductivity of ethylene glycol base fluid and its estimation using Artificial Neural Network for industrial and commercial applications," *J. Saudi Chem. Soc.*, vol. 27, no. 2, 101613, 2023. [CrossRef]
37. X. Tan *et al.*, "Investigation of addition of calcium phosphate ceramic to multilayer scaffold for bone applications with improved mechanical properties: Fuzzy logic analysis," *Ceram. Int.*, vol. 49, no. 5, pp. 8339–8349, 2023. [CrossRef]
38. A. Lefteh, M. Houshmand, M. Khorrampanah, and G. F. Smaisim, "Optimization of Modified Adaptive Neuro-fuzzy Inference System (MANFIS) with artificial bee colony (ABC) algorithm for classification of bone cancer," *Second International Conference on Distributed Computing and High Performance Computing (DCHPC), Qom, Iran, Islamic Republic of*, 2022, pp. 78–81. [CrossRef]
39. T. Goktas, and M. Arkan, "Discerning broken rotor bar failure from low frequency load torque oscillation in DTC induction motor drives," *Trans. Inst. Meas. Control*, vol. 40, no. 1, pp. 279–286, 2018. [CrossRef]
40. A. El Idrissi *et al.*, "Diagnostic de défaut de roulement pour un moteur à induction contrôlé par un réseau neuronal artificiel - Contrôle direct du couple à l'aide de la transformée de Hilbert," *Mathématiques*, vol. 10, no. 22, p. 4258, 2022. [CrossRef]
41. H. Pita, G. Zurita, and A. Villarroel, "Software development firmware system for broken rotor bar detection and diagnosis of induction motor through current signature analysis," *J. Mech. Eng. Sci.*, vol. 14, no. 2, pp. 6917–6933, 2020. [CrossRef]
42. Z. Liu, D. Peng, M. J. Zuo, J. Xia, and Y. Qin, "ASMproved Hilbert–Huang transform with soft sifting stopping criterion and its application to fault diagnosis of wheelset bearings," *ISA Trans.*, 2021. [CrossRef]
43. M. Abdelouhab, A. Senhaji, A. Attar, R. Aboutni, and J. Bouchnaif, "Comparative study of field-oriented control of an induction machine with inter-turn short-circuit in healthy and faulty cases," in *E3S Web of Conf.*, vol. 469, 2023. [CrossRef]
44. S. Mari, G. Bucci, F. Ciancetta, E. Fiorucci, and A. Fioravanti, "Impact of measurement uncertainty on fault diagnosis systems: A case study on electrical faults in induction motors," *Sensors (Basel)*, vol. 24, no. 16, 5263, 2024. [CrossRef]
45. R. Rouaibia, Y. Djeghader, and L. Moussaoui, "Artificial neural network and discrete wavelet transform for inter-turn short circuit and broken rotor bars faults diagnosis under various operating conditions," *Electr. Eng. Electromech.*, vol. 2024, no. 3, pp. 31–37, 2024. [CrossRef]
46. A. El Idrissi, A. Derouich, S. Mahfoud, N. El Ouanjli, H. Chojaa, and A. Chantoufi, "Bearing faults diagnosis by current envelope analysis under direct torque control based on neural networks and fuzzy logic—A comparative study," *Electronics*, vol. 13, no. 16, p. 3195, 2024. [CrossRef]

Dr. Abderrahman El Idrissi is currently a doctoral student at the Higher School of Technology at Sidi Mohamed Ben Abdellah University in Fez, Morocco, he was previously a professor of Industrial Technology at the Ministry of National Education until 2016, before he became an educational planner in the same ministry. He received his master's degree in 2018 from Ibn Tofail University in Kenitra, Morocco, and his bachelor's degree in 2015 from Moulay Ismail University in Meknes. His research interests include fault diagnosis, electrical and electronic engineering, electrical systems modeling, electrical machine control techniques, electric vehicles and wind power. Recently, he has begun reviewing research for international journals and conferences.

Dr. Aziz Derouich obtained his diploma from the Superior School of Technical Teaching of Rabat 1995. Further, he got his Diploma of Superior Studies (DESA) in Electronics, Automatic and Information Processing in 2004 and the Ph.D. degree in computer engineering in 2011 from the "University Sidi Mohamed Ben Abdellah" of Fez. In 2014, he obtained his diploma of Habilitation Research from the Faculty of Science and Technology of Fez. He was a professor of Electricity and Computer Science in "Lycée Technique, El Jadida" from 1995 to 1999 and in "Lycée Technique, Fez" from 1999 to 2011. Since 2011, he is a Professor at the Higher School of Technology, Sidi Mohamed Ben Abdellah University, Fez, Morocco. His research interests include: electrotechnical systems, static converters, electrical machines control, renewable energy, and elearning.

Dr. Said Mahfoud is currently a Professor at the "Higher School of Technology, Sultan Moulay Slimane University, Khenifra, Morocco." He graduated from ENSET of Mohammedia, Morocco, with a licence in electrical engineering in 2012, and from ENSET of Rabat with a master's degree in 2015. He received his Ph.D. in Electrical Engineering from SIDI MOHAMED BEN ABDELLAH University in 2022. From September 2013 to July 2023, he worked as an electrical engineering teacher at the Ministry of Education. His areas of interest are electrical engineering, power electronics, electronic engineering, wind energy, power systems, control systems engineering, design renewable energy, power electronics & drives electrical, power engineering, power systems modelling, reliability engineering, grid integration, photovoltaics systems, smart grid, wind turbines, machines control techniques drives, electric vehicles, machines fault diagnosis, artificial neural network, optimization algorithm, and intelligent control machines, He is serving as a reviewer for international journals and conferences, including *IEEE Transactions on Industrial Electronics*, Access, and others, Elsevier journals on ISA transactions, among others; and many journals in the MDPI.

DR. Najib El Ouanjli is currently a Professor at Department of Applied physics at the "Faculty of Sciences and Techniques, Hassan First University, Settat, Morocco." He received his Ph.D. degree in 2021 from "Sidi Mohammed Ben Abdellah University, Higher School of Technology, Fez, Morocco" and his Master Degree in 2015 from the "Faculty of Sciences Dhar El Mahraz, Fez, Morocco." He was a professor of physics Science Ministry of Education from 2013 to 2021. His research interests are focused on renewable energy systems, electrical & electronics engineering, rotating electric machines, system modeling, control techniques, optimization techniques, fault diagnosis, wind turbines and solar energy. He has published over 48 papers (international journals, book chapters, and conferences/workshops). He is serving as a reviewer for international journals and conferences including as IEEE *Transactions on Industrial Electronics, SN Applied Sciences, Energies and Complex & Intelligent Systems*. He is also a guest editor for special issues in *Energies MDPI* and *Machines MDPI* journals.

Dr. Ahmed Chnatoufi is currently a doctoral student at the Higher School of Technology at Sidi Mohamed Ben Abdellah University in Fez, Morocco, He has been employed as a professor of physical at the Ministry of National Education at the university in Fez, Morocco, since September 2013. He obtained his master's degree in 2015 from the "Faculty of Sciences Dhar El Mahraz, Fez, Morocco". His research interests include electric vehicle, fault Diagnosis, artificial neural network, electrical and electronic engineering, rotating electrical machines, system modelling, and control techniques.

Mohamed I. Mossad received his BSc and MSc degrees from Zagazig University, Egypt, and the PhD degree from Cairo University, Egypt, all in electrical engineering. Currently he is an assistant professor in the Department of Electrical and Electronic Engineering Technology, YIC, KSA. His research interests include power system stability, control and renewable energy. He is the editor-in-chief for *YJES*. He is a regular reviewer for the many IEEE transactions, IET electric power application journal, IET generation transmission and distribution journal, *International Journal of Industrial Electronics and Drives* (IJIED) and *International Journal of Energy Engineering* (IJEE).

APPENDIX

Nomenclatures

$i_{s\alpha}$, $i_{s\beta}$, $i_{r\alpha}$ *and* $i_{r\beta}$	Stator currents and rotor currents in (α, β) plan
$v_{s\alpha}$, $v_{s\beta}$,	Stator voltages and rotor voltages in (α, β) plan
$\Psi_{s\alpha}$, $\Psi_{s\beta}$, $\Psi_{r\alpha}$, *and* $\Psi_{r\beta}$	Stator fluxes and rotor fluxes in (α, β) plan
L_m	Mutual inductance
L_f	Leakage inductance
R_s, R_r	Stator resistors and rotor resistors
p	Pairs of poles number
ω_m	Stator angular speed
Ω	Rotation speed
T_m	Electromagnetic torque
T_r	Load torque
J	Moment of inertia
f	Viscous friction coefficient
n_r	Rotation speed
f_r	Rotation frequency
D_c	Diameter of the cage
D_b	Diameter of a ball
N_b	Number of balls
α	Contact angle
f_s	Supply frequency
f_c	Specific frequency of the fault
f_{Ball}	Specific frequency of bearing ball fault
f_{OR}	Specific frequency of outer race fault
f_{IR}	Specific frequency of inner race fault